ELSEVIER

Chemical Physics 197 (1995) 367–388

Chemical Physics

Superexchange versus sequential long range electron transfer; density matrix pathways in Liouville space

Spiros S. Skourtis, Shaul Mukamel

Department of Chemistry, University of Rochester, Rochester, NY 14627, USA

Received 11 January 1995; in final form 4 May 1995

Abstract

Two important issues in the theory of electron transfer: the competition between superexchange and sequential mechanisms, and the contributions of intermediate bridge states to the propagation from donor to acceptor are addressed by formulating the problem using the density matrix. The evolution of the density matrix allows the introduction of Liouville space pathways. By following the time dependence of the populations and coherences of the system (diagonal and off-diagonal elements of the density matrix), we identify the relevant pathways and the electron transfer mechanism.

1. Introduction

Long range electron transfer reactions are ubiquitous in chemistry. They also play an important role in biological processes such as photosynthesis and oxidative phosphorylation, and their understanding is important for the development of artificial systems that convert light energy into useful chemical energy [1–4]. These reactions involve the transfer of an electron (or hole) from a localized donor state to a localized acceptor state that is spatially well separated from the donor (typically 10–20 Å [5,6]). Due to this separation there is no direct electronic coupling between donor and acceptor, and the coupling is induced by the intervening medium which acts as a "bridge". In biological electron transfer reactions the bridge is a protein or a protein and cofactors.

The superexchange mechanism [7] assumes that the only role of the bridge is to provide virtual orbitals that create an effective electronic coupling between donor and acceptor. This coupling is often computed as follows: The total Hamiltonian of the donor–bridge–acceptor system is reduced to an effective two-state donor–acceptor Hamiltonian by partitioning the total system into donor–acceptor and bridge subspaces [8,9]. The off-diagonal element of this Hamiltonian is interpreted as the effective coupling between donor and acceptor (H_{AD}^{ef}). For weakly coupled donor–acceptor systems the electron transfer process is nonadiabatic and the rate is given by the Fermi golden rule [10–13]:

$$\text{Rate}(\text{D} \rightarrow \text{A}) = \frac{2\pi}{\hbar}(H_{AD}^{ef})^2 \,\text{FC}\,. \tag{1}$$

FC is the Franck–Condon overlap between initial and final vibrational states.

Important questions in long range electron transfer are how the energetics and structure of the bridge affect the rate. The energetics of the bridge influence the strength of the electronic coupling between donor and acceptor and are also relevant to the validity of the superexchange mechanism which depends on the coupling strength between donor, acceptor and bridge eigenstates. The superexchange mechanism ap-

SSDI 0301-0104(95)00167-0

plies when all bridge eigenenergies are sufficiently far from the donor and acceptor energies. It fails as a bridge eigenstate is brought to resonance with the donor and acceptor. In this case additional bridge states are strongly mixed with the donor and acceptor, and an effective two-state Hamiltonian cannot adequately describe the electronic dynamics [14]. A sequential mechanism where the population of the intermediate state may become comparable to the population of the acceptor can then contribute to the rate. This possibility has been discussed for the primary charge separation in bacterial photosynthesis. In this reaction an electron transfers from a Bacteriochlorophyll dimer to a Bacteriopheophytin in 3 ps [15]. Both the donor and the acceptor are embedded in protein and there is a Bacteriochlorophyll monomer between the two [16,17]. The central question is whether the monomer acts as a real or a virtual intermediate [18]. There have been numerous theoretical [19–21], and experimental [22–27] attempts to determine the energies of the electronic states involved, and their coupling to the protein degrees of freedom. However, the monomer energy and its role in the primary charge separation is still an open question [20,21,26,27]. This has led to a wealth of studies on the subject [28–32]. It has also led to the suggestion that both superexchange and sequential mechanisms may contribute to the electron transfer rate [33,34].

Bridge structure is particularly relevant in biological electron transfer reactions. The influence of the protein bridge structure is addressed in the context of the superexchange mechanism by inquiring how many structural elements of the protein contribute significantly to H_{AD}^{ef}. Furthermore, the identity of these structural elements (e.g. α helices, β sheets) is important for understanding biological structure-function relationships. A particularly useful theory for H_{AD}^{ef} in biological electron transfer has been the pathway model [35]. It describes H_{AD}^{ef} in terms of electronic coupling routes through protein sites (states) that "connect" donor to acceptor (electron transfer pathways). This allows the visualization of structure-function relationships. A method for the analysis and visualization of interferences between pathways has also been developed [36]. Due to the fundamental significance of biological electron transfer, both the experimental investigation of protein electron transfer rates [37–39], and the theory of bridge-mediated electron transfer [40,41] have received a considerable attention. Alternative approaches to the pathway model for H_{AD}^{ef} involve more detailed bridge Hamiltonians. One method uses direct inversion of the bridge Green function with Hamiltonian parameters obtained from ionization potentials and ab initio calculations on small molecular systems [42]. Another method [43] implements an initial search for the relevant amino acid residues. These residues are used to define the bridge, which is described by an extended-Huckel Hamiltonian. H_{AD}^{ef} is calculated by inverting the bridge Green function.

For smaller model donor–acceptor systems the effective coupling between donor and acceptor states can be calculated at the ab initio level. The eigenstates and eigenenergies of the entire system are computed, and the coupling is taken to be half the energy splitting between the eigenstates with the dominant donor and acceptor components [44–47]. Pathway analysis is often implemented to identify the type of bonding and antibonding interactions (i.e nearest neighbour, nonnearest neighbour, etc.) that contribute to this energy splitting. This is done by mapping the original Hamiltonian in the eigenstate basis to a tight binding Hamiltonian by transforming to a localized bonding/antibonding orbital basis [45–47].

Currently, pathway analysis is limited to the effective electronic matrix element that is assumed to describe the dominant dynamics only in the superexchange limit. The mechanism is only addressed by looking at the populations of the donor, acceptor, and bridge states. It is therefore desirable to develop a unified framework that can simultaneously address the mechanism and provide a pathway picture for the electron transfer process. This may be accomplished by formulating the problem in terms of the time evolution of the density matrix in Liouville space. Liouville space pathway analysis of electron transfer was first suggested by Sparpaglione and Mukamel [48] who considered the transition from nonadiabatic to adiabatic electron transfer. They showed the close formal analogy between this problem and nonlinear optical spectroscopy. Liouville space pathways were developed for the interpretation of nonlinear susceptibilities and this analogy allowed their direct use in the description of rate processes [49]. Hu and Mukamel [33] formulated the electron transfer problem for the reaction center in Liouville space, including a single bridge state. Their formulation included the cou-

pling to nuclear degrees of freedom and allowed for an arbitrary correlation between the dephasing mechanisms of the donor, acceptor, and intermediate state. They showed that this representation (as opposed to the conventional wavefunction approach) allows the introduction of Liouville space pathways which follow explicitly the evolution of populations and coherences. A Liouville space pathway does not only describe the intermediate states visited in the course of the electron transfer. It also describes how they are visited (e.g. via a superexchange or a sequential mechanism). The competition between the two mechanisms was shown to be formally identical to the branching ratios between Raman and Fluorescence in spontaneous light emission, or between coherent and sequential two photon absorption in pump–probe spectroscopy [50,51]. Mak and coworkers [52] have recently applied the Liouville space diagram analysis of Hu and Mukamel using path integral methods. In the present work we extend the Liouville space analysis to a system with an arbitrary number of bridge states, but without including the nuclear degrees of freedom. A multistate bridge is necessary for the description of many long range electron transfer problems. The present method is suitable for the analysis of the interference between superexchange and sequential mechanisms because it partitions the relevant observable, (the donor–acceptor transition probability), into superexchange and sequential contributions. It can be used to compute the contributions of each mechanism in both the weak, intermediate and strong coupling limits to the bridge.

In Section 2 we introduce the tight binding Hamiltonian of the electron transfer system. To set the stage for the Liouville space analysis, we first relate the time-dependent donor–acceptor transition probability to the corresponding Hilbert space Green function and describe the effective two-state approximation. We demonstrate how this approximation breaks down as the donor and acceptor energies approach the bridge eigenenergies. It then becomes necessary to retain the energy dependence of the effective two-state Hamiltonian or, alternatively, to modify the effective Hamiltonian by including more than two states. The parameters are taken from ab initio calculations on small linear alkyl chains where the donor and acceptor are (Ch_2) p orbitals or σ bonds [45,46]. In Section 3 we introduce the density matrix description of electron transfer in Liouville space. We define the Liouville operator and the Liouville space frequency-domain Green function whose Fourier transform is the time dependent donor–acceptor transition probability. In Section 4 we consider the full time dependent density matrix for the systems studied in Section 2. We analyze the relative importance of the sequential and superexchange mechanisms and identify the bridge states that contribute to each mechanism. This establishes the pathway structure for these systems. In Section 4.1 we calculate the superexchange and sequential contributions to the transition probability. The Liouville space Green function is written in terms of superexchange and sequential effective matrix elements. The purely superexchange Green function is also introduced. It is related to the exact Liouville space Green function through a tetradic scattering matrix [54] that describes the total effect of the sequential contributions. We then study the interference between the superexchange and sequential contributions for the systems of Section 2, using the Liouville space Green functions. Application to systems where the bridge contains an impurity site is made in Section 4.2. We hold the donor (acceptor) energy fixed and bring the energy of the impurity site towards the donor and acceptor energies. Pathway analysis for these systems is done in a localized bridge state representation and the behaviour of all Liouville-space pathways associated with the impurity site is studied. In Appendix A we relate the exact Liouville Green function to the superexchange Green function through the scattering matrix describing the sequential contributions. An alternative definition of the superexchange Green function is provided in Appendix B.

2. Hilbert space description of electron transfer

To set the stage for the Liouville space analysis and to introduce the model and notation, we shall first review the conventional (Hilbert space) formulation of the problem. Consider an N-state system consisting of a donor state, an acceptor state, and $N-2$ bridge states. The Hamiltonian is (Fig. 1)

$$\hat{H} = \hat{H}_0 + \hat{V}, \tag{2}$$

where

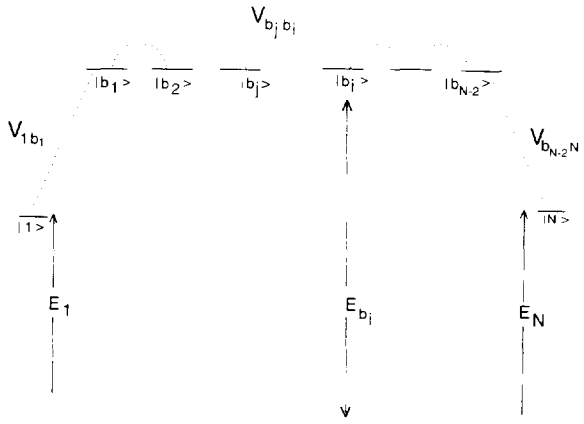

Fig. 1. Tight binding basis used for the N-state donor–bridge–acceptor Hamiltonian. For $V_{b_i,b_j}/(E_{1(N)} - E_{b_i}) < 0$, $(i = 1, N-2)$, the model mimics both electron and hole transfer. In our analysis the localized bridge orbitals model C–C σ bonds, and $N = 8$. The donor and acceptor energies E_1, E_N are varied, as shown in Fig. 2.

$$\hat{H}_0 = \sum_{i=1}^{N-2} E_{b_i}|b_i\rangle\langle b_i| + \sum_{i,j} V_{b_i,b_j}|b_i\rangle\langle b_j| + E_1|1\rangle\langle 1| + E_N|N\rangle\langle N|,$$

$$\hat{V} = \sum_{i=1}^{N-2} V_{1,b_i}|1\rangle\langle b_i| + V_{N,b_i}|N\rangle\langle b_i| + \text{h.c.}$$

$\hat{H}_0$ describes the isolated bridge and donor–acceptor subsystems and $\hat{V}$ is their coupling. $|b_i\rangle$ denote localized bridge orbitals and $|1\rangle$, $|N\rangle$, denote the donor and acceptor states. By diagonalizing the bridge Hamiltonian we can write the Hamiltonian in the form

$$\hat{H}_0 = \sum_{m=1}^{N-2} E_{k_m}|k_m\rangle\langle k_m| + E_1|1\rangle\langle 1| + E_N|N\rangle\langle N| \quad (3)$$

and

$$\hat{V} = \sum_{m=1}^{N-2} \left[\beta_{1k_m}|1\rangle\langle k_m| + \beta_{Nk_m}|N\rangle\langle k_m|\right] + \text{h.c.} \quad (4)$$

$|k_m\rangle$ denote the bridge eigenstates with eigenenergies E_{k_m}. $\beta_{k_m 1}$, $\beta_{k_m N}$ denote the donor–bridge and acceptor–bridge couplings (Fig. 2). The eigenenergies of $\hat{H}$ are denoted $\mathcal{E}_i$.

For a realistic description of a rate process we need to add nuclear (solvent) degrees of freedom which provide dephasing mechanisms and are responsible for the reorganization energy. In this work we focus on the pure electronic system. The incorporation of a bath representing the solvent or nuclear degrees of freedom of the protein can be made using the spectral density or path integral formalism [53]. The system is initially in the donor state and the quantity of interest is the time dependent transition probability to the acceptor state:

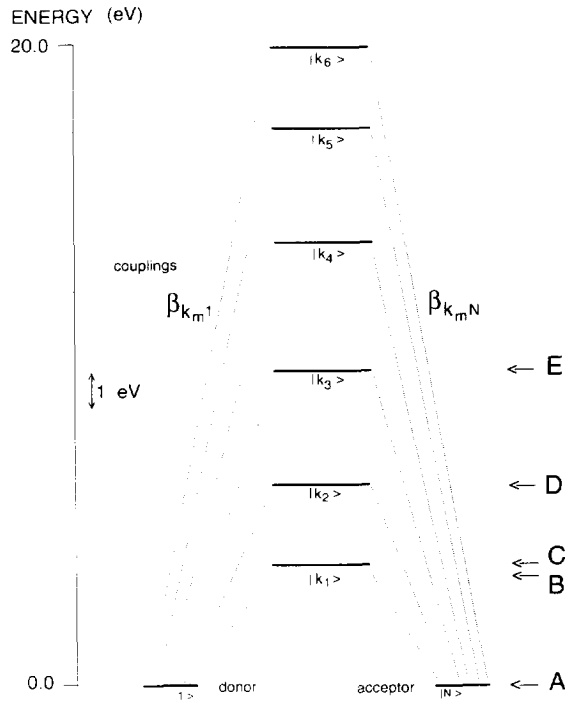

Fig. 2. Same as in Fig. 1 but in bridge eigenstate basis $|k_m\rangle$ for $N = 8$. The relative positions of E_{k_m} and E_1, E_N reflect the energetics of the systems **A–E** (see also Table 1).

Table 1
Parameters used in the variation of donor and acceptor energies through the bridge eigenspectrum. In all cases $E_{b_i} = 11.94$ eV, $V_{b_i,b_{i+1}} = 4.50$ eV, and V_{1,b_1}, $V_{N,b_{N-2}} = 1.37$ eV

System	E_1, (E_N), (eV)	$R_{k_m,i}$, $i = 1, N$	
A	0.0	0.08	$(m = 1)$
B [a]	3.49	0.93	$(m = 1)$
C	3.83	244.40	$(m = 1)$
D	6.33	124.03	$(m = 2)$
E	9.93	110.65	$(m = 3)$

[a] For this system $E_{b_i} - E_1$, $E_{b_i} - E_N = 8.45$ eV, as in Ref. [46].

$$P_{N,1}(t) = |G_{N,1}(t)|^2 , \tag{5}$$

where

$$G_{N,1}(t) = -\frac{1}{2\pi i}\int_{-\infty}^{\infty} dE \exp(-iEt/\hbar) G_{N,1}(E) , \tag{6}$$

and $\hat{G}(E)$ is the Hilbert space retarded Green function,

$$\hat{G}(E) = \frac{1}{E - \hat{H} + i\eta} . \tag{7}$$

$G_{N,1}(E)$ can be calculated by partitioning the total basis set into donor–acceptor (P), and bridge (Q), subspaces, using the following projection operators,

$$P = |1\rangle\langle 1| + |N\rangle\langle N| , \quad Q = \sum_m |k_m\rangle\langle k_m| . \tag{8}$$

One gets

$$P\hat{G}(E)P = P\frac{1}{E - P\hat{H}_0 P - P\hat{H}^{ef}(E)P}P , \tag{9}$$

where the effective donor–acceptor Hamiltonian is

$$P\hat{H}^{ef}(E)P = P\hat{H}Q\frac{1}{E - Q\hat{H}Q}Q\hat{H}P . \tag{10}$$

$Q[E - Q\hat{H}Q]^{-1}Q \equiv \hat{G}_b(E)$ is the bridge Green function [8]. In the bridge eigenstate representation the matrix elements of $P\hat{H}^{ef}(E)P$ are given by

$$H^{ef}_{i,j}(E) = \sum_m \frac{\beta_{ik_m}\beta_{k_m j}}{E - E_{k_m}} , \quad i(j) = 1, N . \tag{11}$$

Eq. (9) for $G_{N,1}(E)$ gives

$$G_{N,1}(E) = H^{ef}_{N,1}(E) \times \left\{ [E - E_1 - H^{ef}_{1,1}(E)][(E - E_N - H^{ef}_{N,N}(E)] - H^{ef}_{N,1}(E)H^{ef}_{1,N}(E) \right\}^{-1} . \tag{12}$$

So far Eq. (12) is exact. The effective two-state picture of electron transfer is obtained by replacing $P\hat{H}^{ef}(E)P$ in Eq. (9) with $P\hat{H}^{ef}(E_{tun})P$, where the tunneling energy E_{tun} is fixed [9]. This gives the effective two-state Green function:

$$P\tilde{G}(E)P \equiv P\frac{1}{E - P\hat{H}_0 P - P\hat{H}^{ef}(E_{tun})P}P . \tag{13}$$

$H^{ef}_{N,1}(E_{tun})$ is the effective coupling that enters the nonadiabatic rate expression (Eq. (1)), and pathways are obtained by writing $H^{ef}_{N,1}(E_{tun})$ in terms of localized bridge states [14,35].

We demonstrate the limitations of the effective two-state picture (see also Ref. [14]) by varying the donor and acceptor energies with respect to the bridge, and comparing $G_{N,1}(E)$ to $\tilde{G}_{N,1}(E)$. We choose parameters from the calculations of Curtiss et al. and Naleway et al. [46] on small linear alkyl chains ($H_2C(CH_2)_{N-2}CH_2$, $N = 4$–8). In these systems the $(CH_2)_{N-2}$ chain is the bridge and the donor and acceptor are the CH_2 p orbitals at each end of the chain. In the Hamiltonian of Eq. (3), we set $N = 8$ and adopt a one dimensional model, keeping only nearest neighbour couplings $V_{b_i,b_{i+1}}$, V_{1,b_1}, and $V_{N,b_{N-2}}$ (Fig. 1). This Hamiltonian is used to model the C–C σ bond backbone of the bridge and the strongest donor (acceptor)–bridge coupling. The $\{|b_i\rangle\}$ represent C–C σ bonds, the $V_{b_i,b_{i+1}}$ represent electronic couplings between adjacent C–C σ bonds, and V_{1,b_1}, $V_{N,b_{N-2}}$ model the strongest couplings between the CH_2 p orbitals and the C–C σ bonds. We use typical values for these parameters [46], i.e. $V_{b_i,b_{i+1}} = 4.5$ eV, and V_{1,b_1}, $V_{N,b_{N-2}} = 1.37$ eV [1].

In the following calculations we vary the donor (acceptor)–bridge energy difference by setting $E_1 = E_N$, and letting E_1, E_N, approach the bridge eigenenergies E_{k_1}, E_{k_2}, and E_{k_3}. We introduce a dimensionless coupling factor between $|1\rangle$, $|N\rangle$, and a bridge eigenstate $|k_m\rangle$, $R_{k_m,j} \equiv |\beta_{k_m j}/(E_{k_m} - E_j)|$, $j = 1, N$. We consider five cases denoted **A**, **B**, **C**, **D**, and **E**. For case **A**, E_1 and E_N are far from all E_{k_m}, and $R_{k_1,1} = R_{k_1,N} = 0.08$. For **B**, E_1 and E_N are chosen such that $E_{b_i} - E_1$, $E_{b_i} - E_N = 8.45$ eV, (in accordance with Ref. [46]), and $R_{k_1,1}$, $R_{k_1,N} = 0.93$. For **C**, **D**, and **E**, $|1\rangle$ and $|N\rangle$ are near resonant to $|k_1\rangle$, $|k_2\rangle$, and $|k_3\rangle$ respectively ($R_{k_m,1}$, $R_{k_m,N} > 100$, $m = 1$–3). The parameters used are summarized in Table 1 and Fig. 2.

Figs. 3 and 4 show $\mathrm{Im}[G_{N,1}(E)]$ and $P_{N,1}(t)$ for these cases. For **A**, $G_{N,1}(E)$ has only two dominant resonances (Fig. 3A). The energy splitting between

[1] The energy difference between the (CH_2) p orbitals and the C–C σ bonds, $(E_{b_i} - E_1, E_{b_i} - E_N)$, is 8.45 eV. If this value is used in the nearest neighbour Hamiltonian, one obtains the correct order of magnitude for the energy splitting between the eigenstates with dominant donor and acceptor components (i.e, ≈ 0.1 eV, as calculated in Ref. [46]).

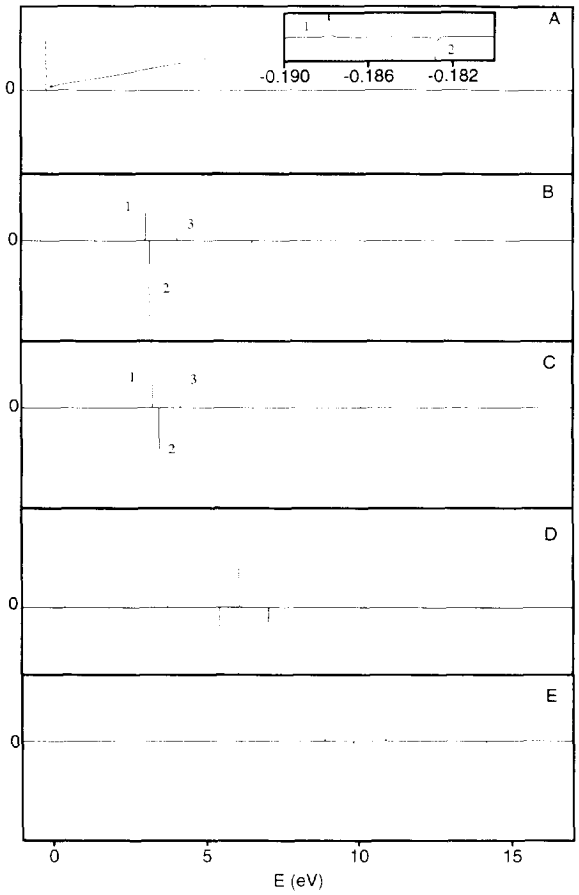

Fig. 3. $\mathrm{Im}[G_{N,1}(E)]$ for systems **A–E**. For **A** there are only two dominant resonances of $G_{N,1}(E)$ at the lowest eigenenergies $\mathcal{E}_1$, $\mathcal{E}_2$. For **B** there appears an additional resonance at the third lowest eigenenergy $\mathcal{E}_3$. For **C** the resonance at $\mathcal{E}_3$ is enhanced with respect to the resonances at $\mathcal{E}_1$ and $\mathcal{E}_2$. **D** and **E** exhibit three large resonances at higher eigenenergies.

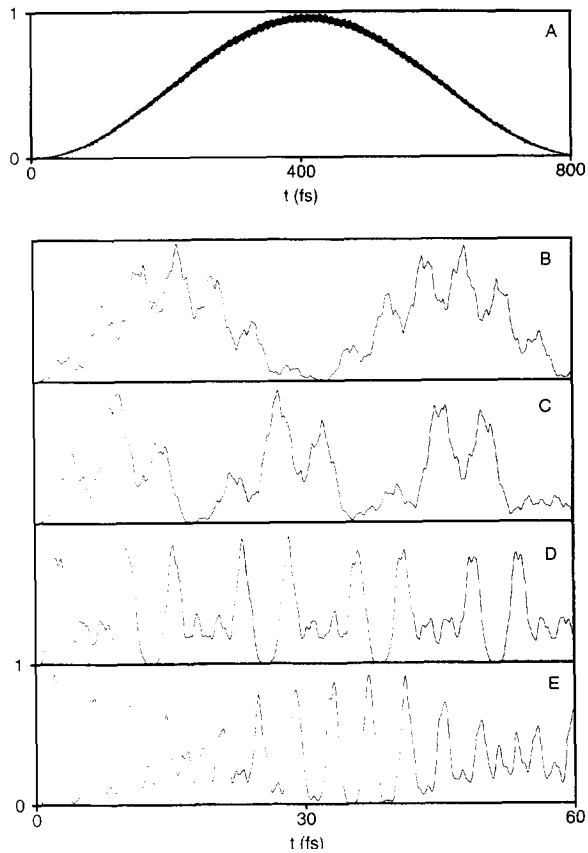

Fig. 4. $P_{N,1}(t)$ for systems **A–E**. For **A** $P_{N,1}(t)$ resembles a sinusoidal oscillation of period $T_{\mathrm{I}} \approx 800$ fs. For **B** and **D** $P_{N,1}(t)$ begins to deviate from a sinusoidal form via a second oscillation of period $T_{\mathrm{II}} \approx 5$ fs. However, in both cases one can distinguish a $\sin^2(t/T_{\mathrm{I}})$ envelope of period $T_{\mathrm{I}} \approx 32.5$ fs (**B**), and $T_{\mathrm{I}} \approx 17.5$ fs (**C**). For **D** and **E** $P_{N,1}(t)$ is very different from a sinusoidal form. As the energetics are changed from **A** to **E**, the periods of the dominant oscillations of $P_{N,1}(t)$ decrease.

these resonances is $\mathcal{E}_2 - \mathcal{E}_1 = 5.04 \times 10^{-3}$ eV. $P_{N,1}(t)$ resembles a $\sin^2(t/T_{\mathrm{I}})$ oscillation where $T_{\mathrm{I}} = h/(\mathcal{E}_2 - \mathcal{E}_1) \approx 800$ fs (Fig. 4A). For **B**, $G_{N,1}(E)$ has three resonances (Fig. 3B). The energy splitting between the two largest is $\mathcal{E}_2 - \mathcal{E}_1 = 0.14$ eV. $P_{N,1}(t)$ still resembles a sinusoidal form (Fig. 4B), but there are much larger deviations from this form as compared to the previous system. One can distinguish two major oscillations of periods $T_{\mathrm{I}} \approx 32.5$ fs, $(T_{\mathrm{I}} = h/(\mathcal{E}_2 - \mathcal{E}_1))$, and $T_{\mathrm{II}} \approx 5$ fs. As $|1\rangle$ and $|N\rangle$ are brought to near resonance with $|k_1\rangle$ (case **C**), the $\mathcal{E}_2 - \mathcal{E}_1$ splitting increases, and the $\mathcal{E}_3$ resonance of $G_{N,1}(E)$ becomes more dominant compared to the previous system (Fig. 3C). The major oscillation of $P_{N,1}(t)$ becomes faster, (T_{I}: 32.5 fs $\rightarrow$ 17.5 fs), and the deviations from the sinusoidal form are more apparent, via the second largest oscillation of period $T_{\mathrm{II}} \approx 5.0$ fs (Fig. 4C). As E_1, E_N are tuned further through the bridge spectrum, (systems **D** and **E**), $G_{N,1}(E)$ attains three large resonances and $P_{N,1}(t)$ deviates significantly from a sinusoidal form (Figs. 3D, 3E, and 4D, 4E).

The structure of $G_{N,1}(E)$ and $P_{N,1}(t)$ for **A** suggests that this system is in the superexchange regime. The dominant dynamics is well approximated by an effective two-state Hamiltonian. For $E_{\mathrm{tun}} = E_1$ one gets

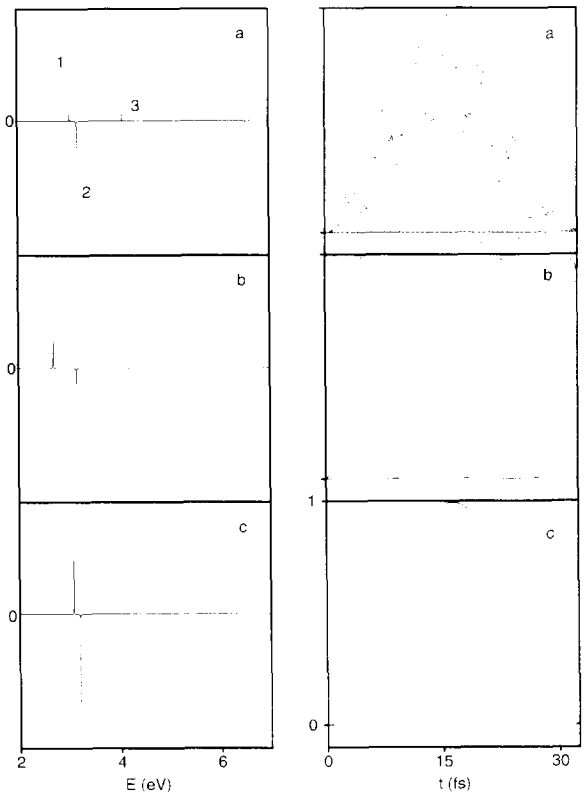

Fig. 5. The effective two-state approximation in both the energy and time domains for system **B**. (a) shows the exact $\mathrm{Im}[G_{N,1}(E)]$ (in the energy regime of the major resonances of $G_{N,1}(E)$), and the exact $P_{N,1}(t)$. One distinguishes two large oscillations in $P_{N,1}(t)$, the largest of period $T_{\mathrm{I}} \approx 32.5$ fs, and the other of period $T_{\mathrm{II}} \approx 5$ fs. Superimposed on the exact $P_{N,1}(t)$ is the difference between the exact and an approximate $P_{N,1}(t)$ (dotted line) obtained by retaining some of the energy dependence in $H^{\mathrm{ef}}_{i,j}(E)$ (i.e. we include E_{k_1}). The difference shows that the approximate $P_{N,1}(t)$ can describe the two major oscillations of the exact. (b) and (c) show the effective two-state approximation in the energy ($\tilde{G}_{N,1}(E)$) and the time ($|\tilde{G}_{N,1}(t)|^2$) domains, for two different E_{tun}. In (b), $E_{\mathrm{tun}} = E_1, E_N$, and the two-state approximation fails to describe the major oscillation of $P_{N,1}(t)$. In (c) the optimal value $E_{\mathrm{tun}} = E_1 - 0.52$ eV is chosen. For this value, $|\tilde{G}_{N,1}(t)|^2$ describes the major oscillation of $P_{N,1}(t)$. However, the two-state approximation cannot reproduce the second largest oscillation of $P_{N,1}(t)$ regardless of the choice of E_{tun}.

$2H^{\mathrm{ef}}_{N,1}(E_1) \approx 1.2(\mathcal{E}_2 - \mathcal{E}_1)$. For **B** the simplest two-state approximation is inadequate even though $|1\rangle$ and $|N\rangle$ are relatively weakly coupled to $|k_1\rangle$ (Table 1). As shown in Figs. 5a, $G_{N,1}(E)$ for **B** has two dominant poles at $\mathcal{E}_1$ and $\mathcal{E}_2$, and $P_{N,1}(t)$ has one dominant oscillation (with period $T_{\mathrm{I}} = h/(\mathcal{E}_2 - \mathcal{E}_1)$). It seems therefore reasonable to approximate this dynamics by an effective two-state Hamiltonian. However, a choice of $E_{\mathrm{tun}} = E_1, E_N$ misses the $\mathcal{E}_1$ residue, overestimates $\mathcal{E}_2 - \mathcal{E}_1$ ($2H^{\mathrm{ef}}_{N,1}(E_1) = 3.4(\mathcal{E}_2 - \mathcal{E}_1)$), and underestimates T_{I}. This is shown by the plots of $\mathrm{Im}[\tilde{G}_{N,1}(E)]$ and $|\tilde{G}_{N,1}(t)|^2$ in Figs. 5b. In this situation it is necessary to vary E_{tun} away from E_1, E_N, in order to get a better approximation for the dominant dynamics [9]. Figs. 5c show $\mathrm{Im}[\tilde{G}_{N,1}(E)]$ and $|\tilde{G}_{N,1}(t)|^2$ for the optimal $E_{\mathrm{tun}} = E_1 - 0.52$ eV. Even better approximations to $P_{N,1}(t)$ are obtained by retaining some of the energy dependence of $H^{\mathrm{ef}}_{ij}(E)$ in $\tilde{G}_{N,1}(E)$. For example, if we pick an energy regime for $H^{\mathrm{ef}}_{ij}(E)$ that contains E_{k_1}, we recover the two largest oscillations of $P_{N,1}(t)$. Fig. 5a shows the difference between the exact $P_{N,1}(t)$ and $P_{N,1}(t)$ obtained by use of this approximation (dotted line). This is equivalent to using an effective three state Hamiltonian with states $|1\rangle$, $|N\rangle$, and $|k_1\rangle$. This approach becomes necessary for cases of near resonance between donor (acceptor) and a bridge eigenstate, where the dominant dynamics are not two-state like (e.g. **C**, **D**, **E** in Fig. 2 and Table 1). For example, in **C**, an effective two-state approximation with $E_{\mathrm{tun}} = E_1, E_N$ greatly overestimates the splitting between the two largest resonances ($2H^{\mathrm{ef}}_{N,1}(E_1) \approx 788(\mathcal{E}_2 - \mathcal{E}_1)$). In **D** and **E** an effective two-state Hamiltonian cannot reproduce the time evolution of $P_{N,1}(t)$ regardless of the choice of E_{tun}.

Evenson and Karplus [55] have analyzed the behaviour of $H^{\mathrm{ef}}_{N,1}(E_{\mathrm{tun}})$ as a function of donor and acceptor energies by tuning E_1, E_N, through the bridge spectrum and setting $E_{\mathrm{tun}} = E_1, E_N$. The above discussion illustrates that such an analysis is not sufficient for a proper description of the dynamics. For situations of near resonance between $|1\rangle$, $|N\rangle$ and $|k_m\rangle$, $H^{\mathrm{ef}}_{N,1}(E^*)$ at a particular energy E^* does not contain enough information to describe the electron transfer dynamics [14], and it becomes necessary to retain the energy dependence of the effective coupling.

3. Density matrix, Liouville space description

We follow the procedure of Hu and Mukamel [33] and switch to a density matrix description of the problem. For a system in a pure state $|\psi(t)\rangle$ the density matrix is defined as $\hat{\rho}(t) \equiv |\psi(t)\rangle\langle\psi(t)|$. For a system

in a mixed state (i.e., a statistical ensemble of states), $\hat{\rho}(t) \equiv \sum_n P_n |\psi_n(t)\rangle\langle\psi_n(t)|$, where P_n is the probability that the system is in state $|\psi_n(t)\rangle$. The expectation value of any observable $\hat{A}$ is given by [56,57]

$$\langle A(t)\rangle = \mathrm{Tr}\{\hat{A}\hat{\rho}(t)\} . \tag{14}$$

The density matrix $\hat{\rho}(t)$ of the system satisfies the Liouville equation

$$\frac{\mathrm{d}}{\mathrm{d}t}\hat{\rho}(t) = -\frac{\mathrm{i}}{\hbar}[\hat{H}, \hat{\rho}(t)] \equiv -\frac{\mathrm{i}}{\hbar}\hat{L}\hat{\rho}(t) , \tag{15}$$

whose solution is

$$\begin{aligned}\hat{\rho}(t) &= \exp(-\mathrm{i}\hat{H}t/\hbar)\hat{\rho}(0)\exp(\mathrm{i}\hat{H}t/\hbar) \\ &\equiv \exp(-\mathrm{i}\hat{L}t/\hbar)\hat{\rho}(0) .\end{aligned} \tag{16}$$

The Liouvillian $\hat{L}$ is given by

$$\hat{L} = \hat{L}_0 + \hat{L}_V . \tag{17}$$

$\hat{L}$, $\hat{L}_0$, $\hat{L}_V$, are defined by their actions on ordinary (Hilbert space) operators $\hat{O}$, i.e.,

$$\begin{aligned}&\hat{L}\hat{O} \equiv [\hat{H}, \hat{O}] , \quad \hat{L}_0\hat{O} \equiv [\hat{H}_0, \hat{O}] , \\ &\hat{L}_V\hat{O} \equiv [\hat{V}, \hat{O}] .\end{aligned} \tag{18}$$

Any ordinary operator $\hat{O}$ in Hilbert space corresponds to a vector in Liouville space denoted by $|O\rangle\rangle$. $\hat{L}$ is a Liouville space operator (also denoted superoperator) acting on the vectors $|...\rangle\rangle$. The scalar product of two vectors corresponding to the Hilbert space operators $\hat{O}_1$, $\hat{O}_2$ is defined by

$$\langle\langle O_1|O_2\rangle\rangle \equiv \mathrm{Tr}\{\hat{O}_1^{\dagger}\hat{O}_2\} . \tag{19}$$

For any pair of Hilbert states $|m\rangle$, $|n\rangle$, we define the Liouville state ket $|mn\rangle\rangle \equiv |m\rangle\langle n|$. Therefore, the Liouville space corresponding to $|1\rangle$, $|N\rangle$, $\{|k_m\rangle\}$, is defined by the vectors $|11\rangle\rangle$, $|NN\rangle\rangle$, $|N1\rangle\rangle$, $|1N\rangle\rangle$, $\{|k_m 1\rangle\rangle\}$, $\{|1k_m\rangle\rangle\}$, $\{|k_m N\rangle\rangle\}$, $\{|Nk_m\rangle\rangle\}$, and $\{|k_n k_m\rangle\rangle\}$ (Fig. 6a).

In the Liouville space picture

$$\begin{aligned}P_{N,1}(t) &= \mathsf{G}_{NN,11}(t) \\ &= -\frac{1}{2\pi\mathrm{i}}\int_{-\infty}^{\infty}\mathrm{d}\omega\,\exp(-\mathrm{i}\omega t)\mathsf{G}_{NN,11}(\omega) ,\end{aligned} \tag{20}$$

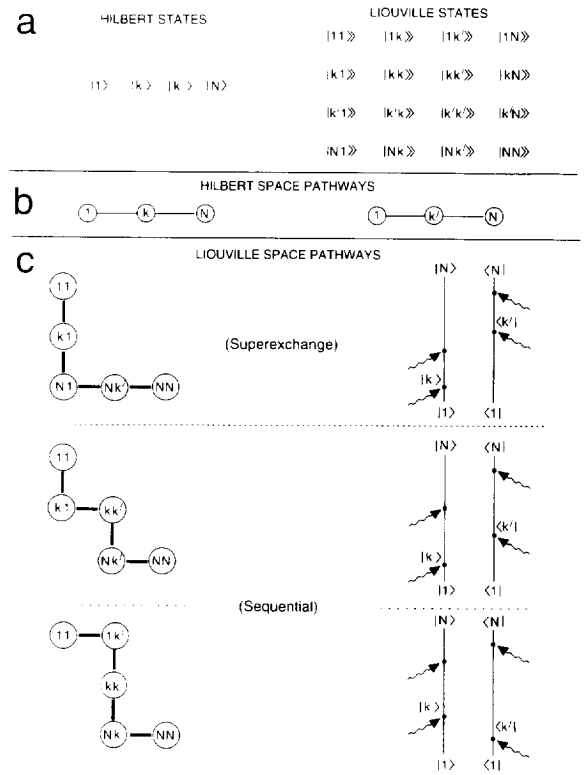

Fig. 6. (a) Liouville states corresponding to Hilbert states: $|1\rangle$, $|k\rangle$, $|k'\rangle$, $|N\rangle$. (b) Hilbert space pathways (to second order in the electronic couplings) through states $|k\rangle$, and $|k'\rangle$. (c) Liouville space pathways through these states (to fourth order in electronic the couplings), and corresponding double sided Feynman diagrams (shown on the right) [33,51]. One can distinguish between superexchange and sequential pathways.

where $\hat{\mathsf{G}}(\omega)$ denotes the Liouville space Green function:

$$\begin{aligned}&\hat{\mathsf{G}}(t) = \theta(t)\exp(-\mathrm{i}\hat{\mathsf{L}}t) , \\ &\hat{\mathsf{G}}(\omega) = \frac{1}{\omega - \hat{\mathsf{L}} + \mathrm{i}\eta} ,\end{aligned} \tag{21}$$

$\omega = E/\hbar$, $\hat{\mathsf{L}} = \hat{L}/\hbar$, and $\mathsf{G}_{ij,kl}(\omega) \equiv \langle\langle ij|\hat{\mathsf{G}}(\omega)|kl\rangle\rangle$. Since $P_{N,1}(t)$ is real, $\mathsf{G}_{NN,11}(-\omega) = -\mathsf{G}^*_{NN,11}(\omega)$. From Eq. (16) it follows that

$$\mathsf{G}_{ij,kl}(\omega) = \frac{\hbar}{2\pi\mathrm{i}}\int \mathrm{d}E\, G_{i,k}(\hbar\omega + E)G^*_{l,j}(E) , \tag{22}$$

where $\hat{G}(E)$ is the Hilbert space Green function (Eq. (7)).

4. Liouville space pathway analysis

The physical picture of the electron transfer process is readily obtained by following the time evolution of all elements $\rho_{ij}(t)$ of the density matrix, assuming that $\hat{\rho}(0) = |1\rangle\langle 1|$. The acceptor population is $P_{N,1}(t) = \rho_{N,N}(t)$. The superexchange mechanism proceeds via the coherence between donor and acceptor given by the matrix elements $\rho_{N,1}(t)$ and $\rho_{1,N}(t)$. The matrix elements involving the bridge eigenstates $|k_m\rangle$ describe bridge populations ($P_{k_m,1}(t) = \rho_{k_m,k_m}(t)$), and bridge coherences ($\rho_{k_m,k_n}(t)$). The sequential mechanism proceeds via these elements. In terms of the Liouville space Green function we have $\rho_{ij}(t) = G_{ij,11}(t)$. One expects that in near resonance situations where the two-state approximation is inadequate, bridge populations and coherences involving the closest (in energy) bridge eigenstate will provide substantial contributions to the sequential mechanism. By following the time evolution of the density matrix elements we can determine which mechanism is dominant.

We first identify the mechanism for the systems considered in Section 2, by comparing $P_{N,1}(t)$, the magnitude of the superexchange matrix element $|G_{N1,11}(t)|$, and the total bridge population $P_{\mathrm{br},1}(t) = \sum_m P_{k_m,1}(t)$. Figs. 7, 8, and 9 show these quantities for cases **A**, **B**, and **C** respectively. For **A**, the amplitude of $P_{\mathrm{br},1}(t)$ is negligible compared to $|G_{N1,11}(t)|$, indicating the dominance of the superexchange mechanism. For **B** (Fig. 8) the amplitude of $P_{\mathrm{br},1}(t)$ is comparable to the amplitude of $|G_{N1,11}(t)|$ (≈ 0.5). The dominant contribution to $P_{\mathrm{br},1}(t)$ comes from the population of the lowest bridge eigenstate $P_{k_1,1}(t)$, as shown in Fig. 8d (amplitude ≈ 0.35). Even though states $|1\rangle$ and $|N\rangle$ are off resonant with respect to $|k_1\rangle$, the sequential mechanism is comparable to the superexchange, and it takes place via $|k_1\rangle$. When E_1 and E_N are tuned near resonant to E_{k_1}, (case **C**, Fig. 9), there is a relative enhancement of $P_{\mathrm{br},1}(t)$ with respect to $|G_{N1,11}(t)|$ (amplitudes ≈ 0.6 , 0.45 respectively). $P_{k_1 1}(t)$ still provides the dominant contribution to $P_{\mathrm{br},1}(t)$ (Fig. 9d). Similar behaviour is seen for systems **D** and **E** (not shown) where $|1\rangle$ and $|N\rangle$ are near resonant to $|k_2\rangle$ and $|k_3\rangle$.

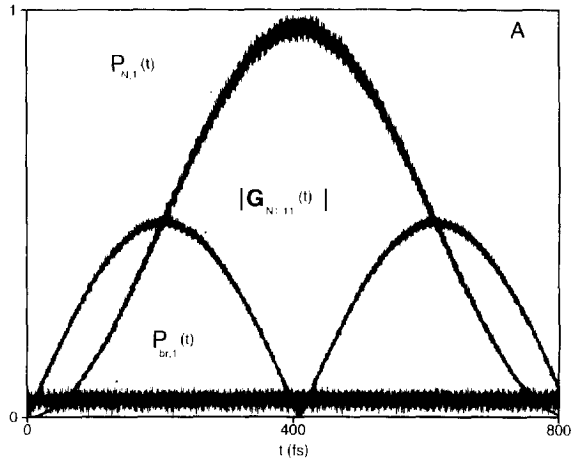

Fig. 7. Comparison of $P_{N,1}(t)$, $|G_{N1,11}(t)|$ (superexchange mechanism), and the total bridge population $P_{\mathrm{br},1}(t)$ (sequential mechanism), for system **A**. $|G_{N1,11}(t)|$ is comparable to $P_{N,1}(t)$, whereas $P_{\mathrm{br},1}(t)$ is negligible. This indicates that electron transfer takes place via a superexchange mechanism.

A more detailed visualization of the mechanism is obtained by displaying the absolute value of all elements of the density matrix $|G_{ij,11}(t)|$ using the localized bridge basis ($i(j) = 1, N, b_i$). These plots reveal the dominant elements of the density matrix. Fig. 10 shows the density matrix for the superexchange system **A**, at different times spanning the period of the major oscillation of $P_{N,1}(t)$. From this plot it is apparent that the amplitudes of $|G_{b_i,b_j,11}(t)|$ are negligible at all times. The dominant matrix elements are $|G_{11,11}(t)| = P_{1,1}(t)$, $|G_{N1,11}(t)|$, and $|G_{NN,11}(t)| = P_{N,1}(t)$, indicating the applicability of the superexchange mechanism. The other matrix elements contributing to this mechanism are $|G_{b_i1,11}(t)|$, and $|G_{b_iN,11}(t)|$ ($i = 1, N-2$). Fig. 11 shows a similar plot of all $|G_{ij,11}(t)|$ ($i(j) = 1, N, b_i$) for system **B**, at different times spanning the period of the major oscillation of $P_{N,1}(t)$ ($T_{\mathrm{I}} \approx 32.5$ fs). The times chosen correspond to the maxima and minima of the second largest oscillation of $P_{N,1}(t)$ (period $T_{\mathrm{II}} \approx 5$ fs), that causes deviations from the sinusoidal form. One sees a relative enhancement of all $|G_{b_ib_j,11}(t)|$, $|G_{b_i1,11}(t)|$, and $|G_{b_iN,11}(t)|$, with respect to $|G_{11,11}(t)|$, $|G_{N1,11}(t)|$, and $|G_{NN,11}(t)|$. This is seen at times $t = 5$ fs, $t = 9.5$ fs, and $t = 14$ fs. There is not a particular bridge site that dominates.

To identify the bridge eigenstates contributing to the processes shown in Fig. 11, we plot in Fig. 12 all $|G_{ij,11}(t)|$ in the bridge eigenstate representation (i.e., $i(j) = 1, N, k_m$). The plots show that at the earlier times $t = 5$–9.5 fs, there is substantial

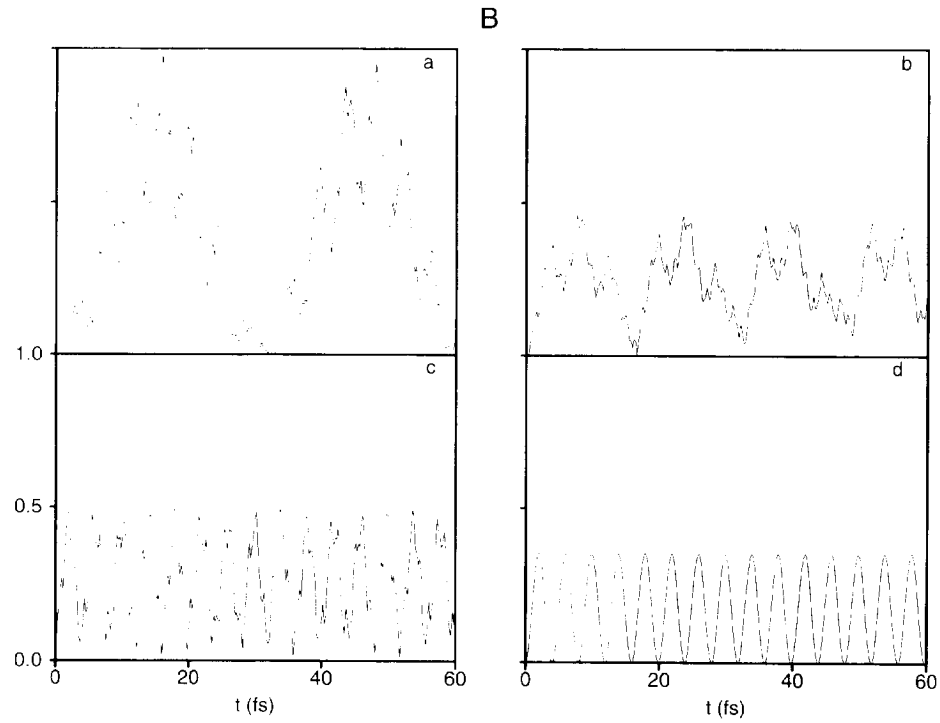

Fig. 8. Comparison of $P_{N,1}(t)$ (**a**), $|G_{N1,11}(t)|$ (b), $P_{\mathrm{br},1}(t)$ (c), and $P_{k_1,1}(t)$ (d), for system B. $|G_{N1,11}(t)|$ and $P_{\mathrm{br},1}(t)$ are of the same amplitude (≈ 0.5), and are both comparable to $P_{N,1}(t)$. This indicates the coexistence of superexchange and sequential mechanisms. Most of the sequential mechanism is primarily due to the eigenstate $|k_1\rangle$, as seen from $P_{k_1,1}(t)$.

amplitude in $|G_{k_1 1,11}(t)|$ and $|G_{k_1 k_1,11}(t)|$ (as compared to $|G_{11,11}(t)|$, $|G_{N1,11}(t)|$ and $|G_{NN,11}(t)|$). At later times t = 9.5–14.0 fs we observe a buildup of amplitude in $|G_{k_1 N,11}(t)|$. The other matrix elements that are smaller but not negligible compared to $|G_{k_1 1,11}(t)|$, $|G_{k_1 k_1,11}(t)|$, and $|G_{k_1 N,11}(t)|$, involve $|k_2\rangle$ (e.g. $|G_{k_2 k_1,11}(t)|$, $|G_{k_2 k_2,11}(t)|$, $|G_{k_2 1,11}(t)|$, $|G_{k_2 N,11}(t)|$). This figure indicates that the deviation of $P_{N,1}(t)$ from the sinusoidal form (via the second largest oscillation of period T_{II}), arises mainly from the participation of $|k_1\rangle$. These effects are further enhanced as E_1 and E_N approach E_{k_1} (not shown).

4.1. Superexchange and sequential components of $G_{NN,11}(\omega)$

We now compute the contributions of the superexchange and sequential mechanisms to $P_{N,1}(t)$ or $G_{NN,11}(\omega)$. There is no unique way to accomplish this goal. A reasonable classification which will be adopted here (see Appendix A), is to define as superexchange any process contributing to the transition from $|11\rangle\rangle$ to $|NN\rangle\rangle$ that visits the Liouville states $|N1\rangle\rangle$ and $|1N\rangle\rangle$. Such a process may also involve states $|k_m 1\rangle\rangle$, $|k_m N\rangle\rangle$, and $|k_m k_n\rangle\rangle$ (and their hermitian conjugates) as intermediates. All remaining processes are denoted sequential. An alternative definition of superexchange is given in Appendix B. According to this definition any process contributing to the transition from $|11\rangle\rangle$ to $|NN\rangle\rangle$ that does not visit bridge populations and coherences ($|k_m k_n\rangle\rangle$) is classified as superexchange.

Since we are interested in level populations we will express $G_{NN,11}(\omega)$ in terms of the 2×2 matrix $P\hat{G}(\omega)P$, where P is the Liouville space projection operator

$$P = |11\rangle\rangle\langle\langle 11| + |NN\rangle\rangle\langle\langle NN| . \tag{23}$$

In Appendix A we derive the following expression for $PG(\omega)P$:

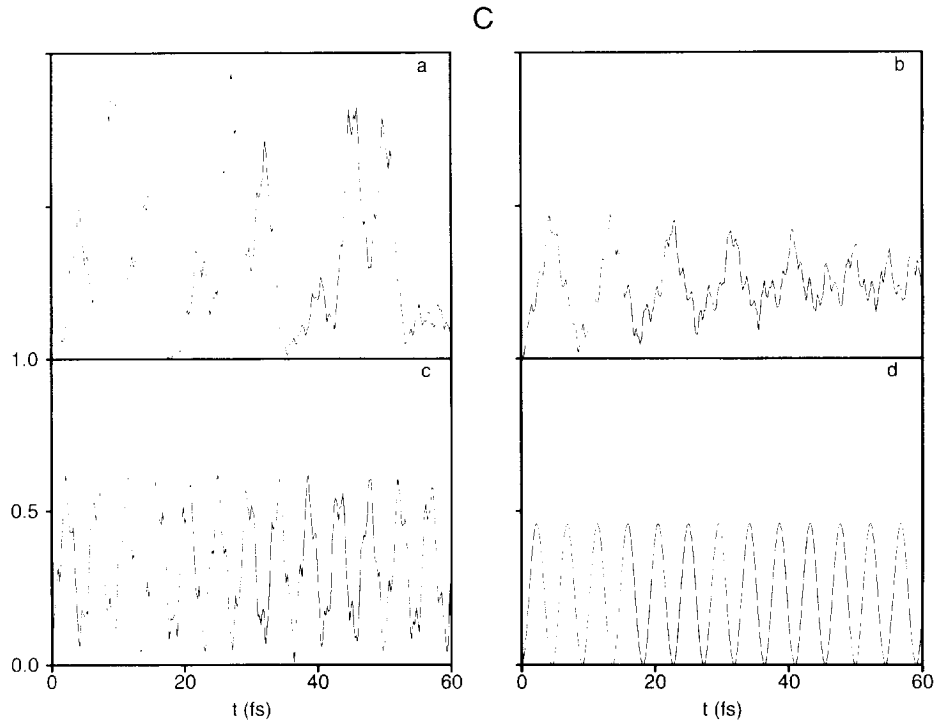

Fig. 9. Same as in Fig. 8 but for system C. $P_{\mathrm{br},1}(t)$ has larger amplitude than $|G_{N1,11}(t)|$ (≈ 0.6, 0.45 respectively), and both are comparable to $P_{N,1}(t)$. Therefore, the superexchange and sequential mechanisms compete for this system. The enhancement of the sequential mechanism is due to the near resonance between $|1\rangle$, $|N\rangle$ and $|k_1\rangle$. This is reflected in $P_{k_1,1}(t)$, which provides most of the sequential contribution.

$$P\hat{G}(\omega)P = P\frac{1}{w - P\hat{L}^{\mathrm{ef}}(\omega)P - P\hat{\Sigma}(\omega)P}P, \quad (24)$$

where $P\hat{\Sigma}(\omega)P$ is the superexchange contribution (involves states $|N1\rangle\rangle$, $|1N\rangle\rangle$) and $P\hat{L}^{\mathrm{ef}}(\omega)P$ is the sequential contribution (does not involve these states). Expressions for $P\hat{\Sigma}(\omega)P$ and $P\hat{L}^{\mathrm{ef}}(\omega)P$ in terms of the bridge eigenstates $|k_m\rangle$ are given in the appendix (Eqs. (A.7), (A.6)). The pathways contributing to $P\hat{\Sigma}(\omega)P$ and $P\hat{L}^{\mathrm{ef}}(\omega)P$ to lowest order in perturbation theory in the system/bridge coupling are shown in Fig. 6c.

We now define the superexchange Green function (which is considered as the "zeroth order" Green function in our analysis), by retaining only $P\hat{\Sigma}(\omega)P$ in the denominator of Eq. (24):

$$P\hat{G}^{\mathrm{sup}}(\omega)P \equiv P\frac{1}{\omega - P\hat{\Sigma}(\omega)P}P. \quad (25)$$

The matrix element of the superexchange Green function describing electron transfer is given by

$$G^{\mathrm{sup}}_{NN,11}(\omega) = \Sigma_{NN,11}(\omega) \times\Big\{ \big[\omega - \Sigma_{11,11}(\omega)\big]\big[\omega - \Sigma_{NN,NN}(\omega)\big] - \Sigma_{NN,11}(\omega)\Sigma_{11,NN}(\omega)\Big\}^{-1}. \quad (26)$$

The total $G_{NN,11}(\omega)$ is then expressed in terms of $P\hat{G}^{\mathrm{sup}}(\omega)P$ and the tetradic scattering matrix $P\hat{T}^{\mathrm{seq}}(\omega)P$ arising from the sequential matrix elements $P\hat{L}^{\mathrm{ef}}(\omega)P$:

$$G_{NN,11}(\omega) = G^{\mathrm{sup}}_{NN,11}(\omega) + \sum_{\alpha\beta,\gamma\delta=11,NN} G^{\mathrm{sup}}_{NN,\alpha\beta}(\omega)T^{\mathrm{seq}}_{\alpha\beta,\gamma\delta}(\omega)G^{\mathrm{sup}}_{\gamma\delta,11}(\omega), \quad (27)$$

where $T^{\mathrm{seq}}_{\alpha\beta,\gamma\delta}(\omega)$ are given in Appendix A.

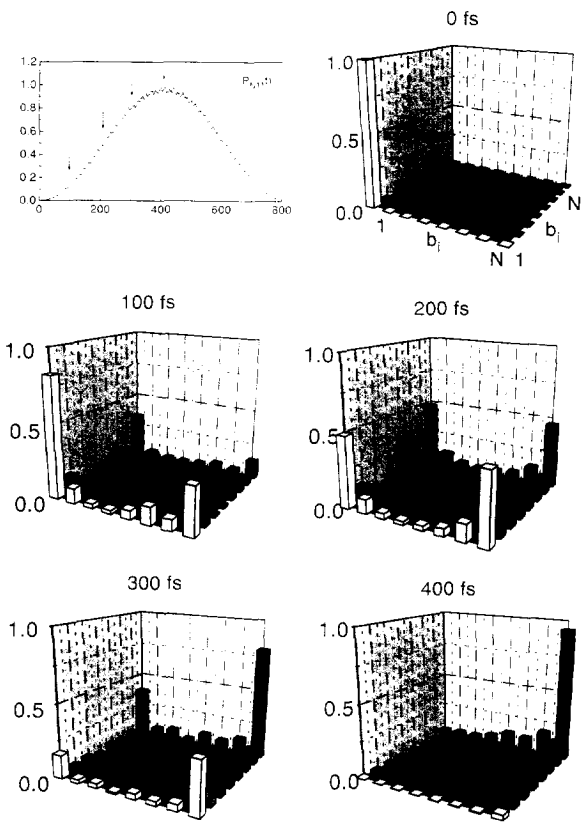

Fig. 10. The absolute value of the density matrix in the localized bridge basis, (i.e. $|G_{ij,11}(t)|$ for $i(j) = 1, N, b_i$), for system **A**. The plots are at $t = 0$ and at several other times spanning the period of the major oscillation of $P_{N,1}(t)$ (indicated by the arrows). The x and y axis of each plot label i and j in $|G_{ij,11}(t)|$, using the sequence 1, b_1, ... b_{N-2}, N. The z axis shows $|G_{ij,11}(t)|$. The dominant matrix elements are $|G_{11,11}(t)| = P_{1,1}(t)$, $|G_{N1,11}(t)|$, and $|G_{NN,11}(t)| = P_{N,1}(t)$. The amplitudes of $|G_{b_ib_j,11}(t)|$ are negligible at all times, indicating the dominance of the superexchange mechanism.

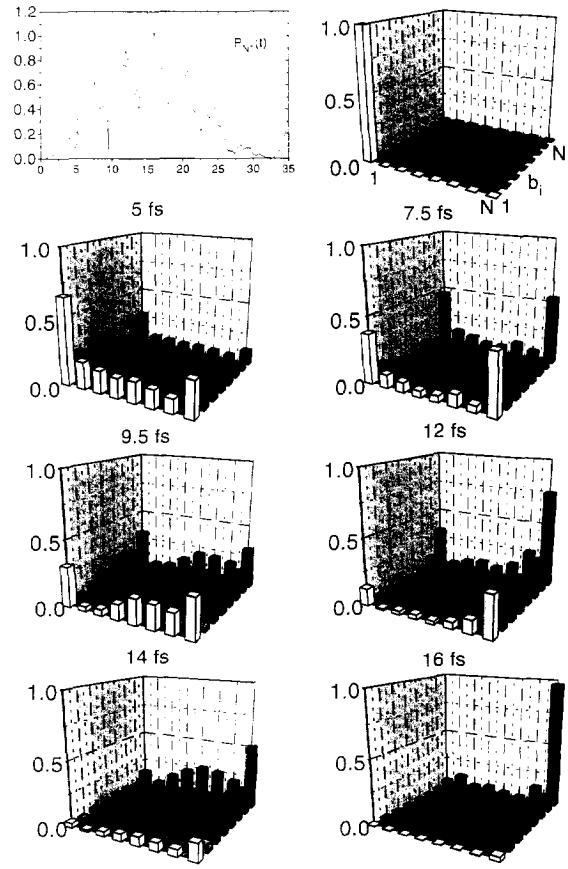

Fig. 11. Same as in Fig. 10 but for system **B**. The plots are at $t = 0$ and at several other times spanning the period of the major oscillation of $P_{N,1}(t)$. The times chosen correspond to the maxima and minima of the second largest oscillation of $P_{N,1}(t)$. The x and y axis of each plot label i and j in $|G_{ij,11}(t)|$, using the sequence 1, b_1, ... b_{N-2}, N. Compared to Fig. 10, one sees a relative enhancement of $|G_{b_ib_j,11}(t)|$ with respect to $|G_{11,11}(t)|$, $|G_{N1,11}(t)|$, and $|G_{NN,11}(t)|$. The enhancement is seen at $t = 5$ fs, $t = 9.5$ fs and $t = 14$ fs, when the second largest oscillation of $P_{N,1}(t)$ reaches its minima.

The superexchange Green functions $G^{sup}_{NN,11}(\omega)$ and $G^{sup}_{NN,11}(t)$ are shown in Figs. 13, 14, and 15 for systems **A**, **B**, and **C** respectively. They are compared to the total $G_{NN,11}(\omega)$ and to $G_{NN,11}(t) = P_{N,1}(t)$ in order to obtain the sequential contributions. We first consider the superexchange system **A**. Fig. 13a shows $\mathrm{Im}[G_{NN,11}(\omega)]$ over a frequency regime that contains the dominant resonances of $G_{NN,11}(\omega)$. $G_{NN,11}(\omega)$ has three major resonances, one at $\omega_0 = 0$ s^{-1}, and the others at $\pm\omega_1$, where $\omega_1 = 7.7 \times 10^{12}$ s^{-1} (only $\omega \geqslant 0$ is shown since $\mathrm{Im}[G_{NN,11}(\omega)]$ is even with respect to ω). These resonances give rise to the major oscillation of $P_{N,1}(t)$ as is demonstrated by taking the Fourier transform of $G_{NN,11}(\omega)$ in this frequency regime (Fig. 13b). An oscillation of approximately unit amplitude and period $T_1 = 2\pi/\omega_1 \approx$ 800 fs is obtained (compare with Fig. 4A which shows the total $P_{N,1}(t)$). For this system $G^{sup}_{NN,11}(\omega)$ gives a good approximation to $G_{NN,11}(\omega)$. In Fig. 13a (superimposed on $\mathrm{Im}[G_{NN,11}(\omega)]$), we show $\mathrm{Im}[G_{NN,11}(\omega) - G^{sup}_{NN,11}(\omega)]$. $G^{sup}_{NN,11}(\omega)$ gets the res-

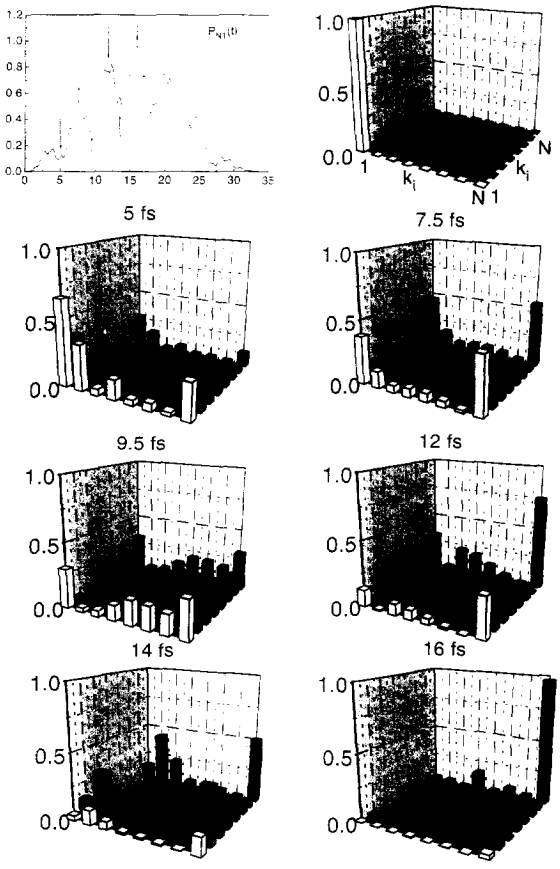

Fig. 12. System **A**. Plots of the absolute value of the density matrix in the bridge eigenstate basis, (i.e. $|G_{ij,11}(t)|$ for $i(j) = 1, N, k_m$). The plots are at $t = 0$ and at the maxima and minima of the second largest oscillation of $P_{N,1}(t)$. The x and y axis of each plot label i and j in $|G_{ij,11}(t)|$, using the sequence 1, k_1, ... k_{N-2}, N. The z axis gives the value of each $|G_{ij,11}(t)|$. The largest matrix elements are $|G_{11,11}(t)|$, $|G_{N1,11}(t)|$, $|G_{NN,11}(t)|$, $|G_{k_1 1,11}(t)|$, $|G_{k_1 k_1,11}(t)|$, and $|G_{k_1 N,11}(t)|$. The buildup of $|G_{k_1 1,11}(t)|$ takes place at the earlier times (e.g. $t = 5$ fs), whereas $|G_{k_1 N,11}(t)|$ becomes significant at later times (e.g. $t = 14$ fs). These plots indicate the participation of $|k_1\rangle$ in both superexchange and sequential mechanisms.

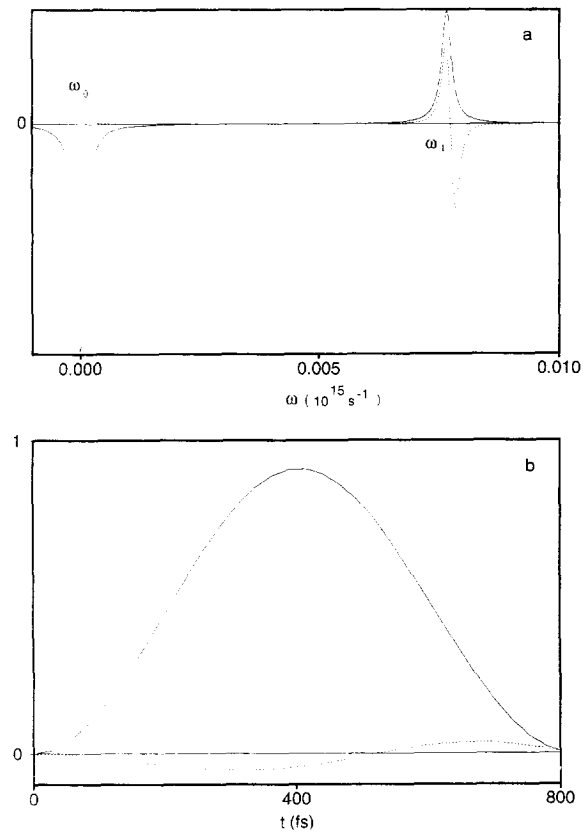

Fig. 13. System **A**. (a) $\mathrm{Im}[G_{NN,11}(\omega)]$ and $\mathrm{Im}[G_{NN,11}(\omega) - G^{\mathrm{sup}}_{NN,11}(\omega)]$ (dotted line), in the frequency regime containing the major resonances of $G_{NN,11}(\omega)$. Since both $\mathrm{Im}[G_{NN,11}(\omega)]$ and $\mathrm{Im}[G^{\mathrm{sup}}_{NN,11}(\omega)]$ are even with respect to ω, only $\omega \geqslant 0$ is shown. (b) $G_{NN,11}(t)$ obtained by Fourier transforming $G_{NN,11}(\omega)$ shown in (a), and $G_{NN,11}(t) - G^{\mathrm{sup}}_{NN,11}(t)$ (dotted line). The plot of $\mathrm{Im}[G_{NN,11}(\omega) - G^{\mathrm{sup}}_{NN,11}(\omega)]$ indicates that $G^{\mathrm{sup}}_{NN,11}(\omega)$ gets the position of the resonance at ω_0 (slightly overestimating its magnitude), and slightly overestimates the position of the resonance at ω_1. $G_{NN,11}(t) - G^{\mathrm{sup}}_{NN,11}(t)$ is small compared to $G_{NN,11}(t)$ indicating that $G^{\mathrm{sup}}_{NN,11}(t)$ gives a good approximation to $G_{NN,11}(t)$.

onance of $G^{\mathrm{sup}}_{NN,11}(\omega)$ at ω_0 and slightly overestimates the position of the resonance at ω_1. Fig. 13b shows $G_{NN,11}(t) - G^{\mathrm{sup}}_{NN,11}(t)$ superimposed on $G_{NN,11}(t)$.

We next consider system **B**, whose energetics are obtained from Ref. [46]. $G_{NN,11}(\omega)$ has seven major resonances, four of which are shown in Fig. 14a (for $\omega \geqslant 0$). These resonances ($\omega_0 = 0.0$ s^{-1}, $\omega_1 = 2 \times 10^{14}$ s^{-1}, $\omega_2 = 1.37 \times 10^{15}$ s^{-1}, $\omega_3 = 1.58 \times 10^{15}$ s^{-1}), give rise to the dominant oscillations of $P_{N,1}(t)$. These oscillations are identified by Fourier transforming $G_{NN,11}(\omega)$ over this frequency range ($G_{NN,11}(t)$ in Fig. 14a). The major period of $G_{NN,11}(t)$ is $T_1 \approx 2\pi/\omega_1$. For this system the superexchange mechanism does not completely describe the dominant dynamics. Figs. 14b show $\mathrm{Im}[G^{\mathrm{sup}}_{NN,11}(\omega)]$ in the same frequency regime and its Fourier transform $G^{\mathrm{sup}}_{NN,11}(t)$. $G^{\mathrm{sup}}_{NN,11}(\omega)$ overestimates the magnitude of the resonance at ω_0 and over-

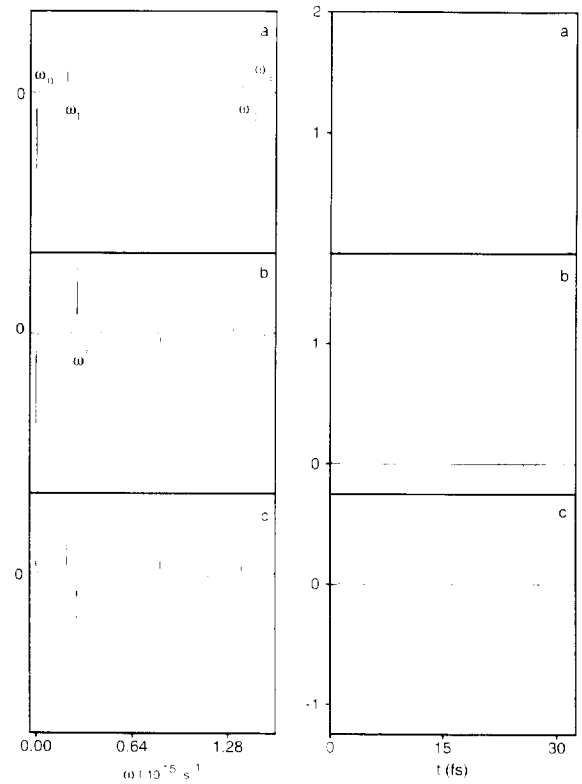

Fig. 14. System **B**. (a) $\mathrm{Im}[G_{NN,11}(\omega)]$ (in the frequency regime of the major resonances of $G_{NN,11}(\omega)$), and its Fourier transform $G_{NN,11}(t)$. The plot of $G_{NN,11}(t)$ indicates that the resonances of $G_{NN,11}(\omega)$ at ω_0, $\pm\omega_1$, $\pm\omega_2$, and $\pm\omega_3$, give rise to the two major oscillations of $P_{N,1}(t)$ of periods $T_{\mathrm{I}} \approx 32.5$ fs and $T_{\mathrm{II}} \approx 5$ fs. (b) $\mathrm{Im}[G^{\mathrm{sup}}_{NN,11}(\omega)]$ (in the same frequency regime as in (a)), and its Fourier transform $G^{\mathrm{sup}}_{NN,11}(t)$. (c) $\mathrm{Im}[G_{NN,11}(\omega) - G^{\mathrm{sup}}_{NN,11}(\omega)]$, and its Fourier transform $G_{NN,11}(t) - G^{\mathrm{sup}}_{NN,11}(t)$. $G^{\mathrm{sup}}_{NN,11}(\omega)$ gets the major resonances of $G_{NN,11}(\omega)$ at ω_0 and $\pm\omega_1$. However, it slightly overestimates the position of the resonance at $\pm\omega_1$ ($\pm\omega'$). This is reflected in $G^{\mathrm{sup}}_{NN,11}(t)$ which displays one oscillation of amplitude $\gtrsim 1$, (as does $G_{NN,11}(t)$), whose period is smaller than the period of the major oscillation of $G_{NN,11}(t)$ (i.e., $T' \approx 20$ fs versus $T_{\mathrm{I}} \approx 32.5$ fs).

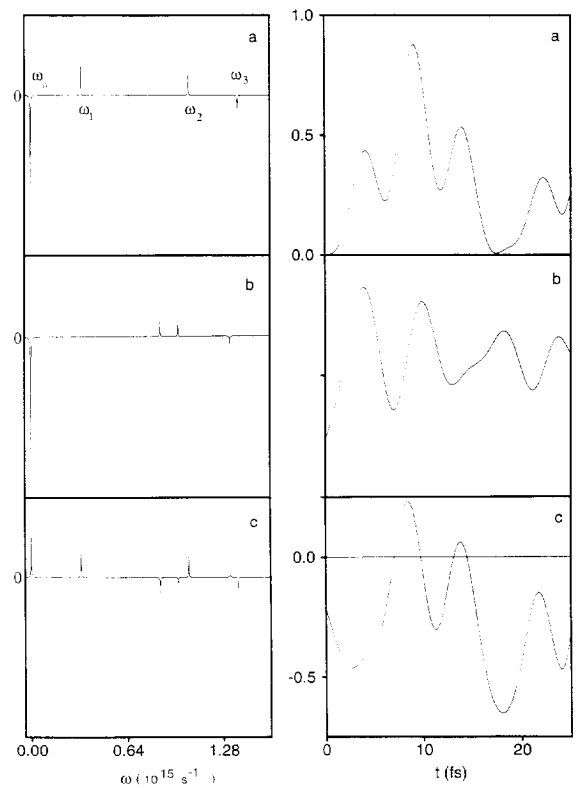

Fig. 15. System **C**. (a) $\mathrm{Im}[G_{NN,11}(\omega)]$ (in the frequency regime of the major resonances of $G_{NN,11}(\omega)$), and its Fourier transform $G_{NN,11}(t)$. $G_{NN,11}(t)$ displays the two major oscillations of $P_{N,1}(t)$ of periods $T_{\mathrm{I}} \approx 17.5$ fs and $T_{\mathrm{II}} \approx 5$ fs. These oscillations arise from the resonances of $G_{NN,11}(\omega)$ at ω_0, $\pm\omega_1$, $\pm\omega_2$, and $\pm\omega_3$. (b) $\mathrm{Im}[G^{\mathrm{sup}}_{NN,11}(\omega)]$ (in the same frequency regime as in (a)), and its Fourier transform $G^{\mathrm{sup}}_{NN,11}(t)$. (c) $\mathrm{Im}[G_{NN,11}(\omega) - G^{\mathrm{sup}}_{NN,11}(\omega)]$, and its Fourier transform $G_{NN,11}(t) - G^{\mathrm{sup}}_{NN,11}(t)$. $G^{\mathrm{sup}}_{NN,11}(\omega)$ gets the resonance of $G_{NN,11}(\omega)$ at ω_0, but completely misses the one at $\pm\omega_1$. This is reflected in $G^{\mathrm{sup}}_{NN,11}(t)$ which does not display an oscillation of amplitude ≈ 1 and of period ≈ 17.5 fs. For this system, the sequential contribution is essential to the description of $P_{N,1}(t)$.

estimates the magnitude and position of the second largest resonance at ω_1 ($\omega_1' = 2.7 \times 10^{14}\ \mathrm{s}^{-1}$). This is shown by the plot of $\mathrm{Im}[G_{NN,11}(\omega) - G^{\mathrm{sup}}_{NN,11}(\omega)]$ in Fig. 14c. $G^{\mathrm{sup}}_{NN,11}(t)$ consists of a dominant oscillation that misses the period of the dominant oscillation of $P_{N,1}(t)$ (its period is approximately $0.7T_{\mathrm{I}}$). This system is not purely superexchange but exhibits an interference between superexchange and sequential mechanisms. The sequential contributions in the time domain are shown in Fig. 14c.

The sequential contribution to $P_{N,1}(t)$ is further enhanced for system **C** for which $|1\rangle$ and $|N\rangle$ are are near resonant to $|k_1\rangle$. Figs. 15a show the the dominant resonances of $G_{NN,11}(\omega)$ ($\omega_1 = 3.2 \times 10^{14}\ \mathrm{s}^{-1}$, $\omega_2 = 1.05 \times 10^{15}\ \mathrm{s}^{-1}$ and $\omega_3 = 1.37 \times 10^{15}\ \mathrm{s}^{-1}$), which give rise to the dominant oscillations of $P_{N,1}(t)$ ($G_{NN,11}(t)$ in Fig. 15a). For this system $G^{\mathrm{sup}}_{NN,11}(\omega)$ completely misses the largest resonance of $G_{NN,11}(\omega)$ at ω_1 (see $\mathrm{Im}[G^{\mathrm{sup}}_{NN,11}(\omega)]$ and $\mathrm{Im}[G^{\mathrm{sup}}_{NN,11}(\omega) - G^{\mathrm{sup}}_{NN,11}(\omega)]$ in

Figs. 15b, 15c). This is reflected in the time domain, where $G^{sup}_{NN,11}(t)$ completely misses the major oscillation of $P_{N,1}(t)$ of period $T_1 \approx 17.5$ fs (Figs. 15b, 15c). This system shows stronger interference between the superexchange and sequential mechanisms.

From Figs. 14 and 15 we see that the magnitudes of $G^{sup}_{NN,11}(t)$ and $G_{NN,11}(t) - G^{sup}_{NN,11}(t)$ are comparable to $G_{NN,11}(t)$, indicating substantial superexchange and sequential contributions. However $G^{sup}_{NN,11}(t)$ does not have the properties of a probability. For **B**, $G^{sup}_{NN,11}(t)$ attains negative values and values greater than 1 (Fig. 14b). For **C**, $G^{sup}_{NN,11}(0) > 0$ (Fig. 15b). This means that when both superexchange and sequential mechanisms are substantial, they strongly interfere.

4.2. *Pathway analysis for a bridge with an impurity*

A comparison of $P_{N,1}(t)$ for the different systems in Figs. 3 and 4 indicates a decrease in the period of the major oscillation of $P_{N,1}(t)$ as E_1, E_N, approach a bridge eigenenergy. This suggests that the period of the main oscillation of $P_{N,1}(t)$ can also be reduced by introducing a bridge impurity site $|b_{im}\rangle$ whose energy is closer to E_1, E_N. The reduction is possible if $|b_{im}\rangle$ creates an impurity bridge eigenstate $|k_{im}\rangle$ with $R_{k_{im},1}$, $R_{k_{im},N} \gtrsim 1.0$, (i.e, $|k_{im}\rangle$ is near resonant to $|1\rangle$, $|N\rangle$). The impurity site can be interpreted as a part of a bridge containing π electron orbitals (as opposed to a majority of σ electron orbitals). There has been speculation for some time about the role of such orbitals in chemical [58] and biological (via aromatic aminoacids) [41,59] electron transfer. Although there is some evidence that such orbitals enhance the rate in small systems [60], their role in protein electron transfer is not clear [41,59].

In the following calculations we use the superexchange system **A** as a reference ($E_1 = E_N = 0$, $E_{b_i} = 11.94$ eV), and create three impurity systems by changing the energy of $|b_3\rangle$. These systems are denoted **I1**, **I2**, and **I3**. The impurity energies are: $E_{b_3} \approx 2(E_{b_i} - E_1)/3$ (for I1), $E_{b_3} \approx (E_{b_i} - E_1)/3$ (for I2), and $E_{b_3} = E_1, E_N$ (for I3). E_{b_i} are the energies of the remaining bridge sites which, together with the electronic couplings, are kept constant as E_{b_3} is varied. The parameters for the reference system and the three impurity systems are shown in Table 2.

Fig. 16 shows $P_{N,1}(t)$ for the reference and the three impurity systems. For **I1** $P_{N,1}(t)$ shows one major os-

Table 2
Parameters used in the variation of the impurity energy at $|b_3\rangle$. In all cases $E_{b_i} = 11.94$ eV for $i \neq 3$, $V_{b_i,b_{i+1}} = 4.50$ eV, V_{1,b_1}, $V_{N,b_{N-2}} = 1.37$ eV, and $E_1 = E_N = 0$

System	E_{b_3} (eV)	$R_{k_{im},1}$	$R_{k_{im},N}$
A [a]	11.94	0.08	0.08
I1	7.94	0.12	0.07
I2	3.94	4.05	1.82
I3	0.0	0.04	0.01

[a] Reference system.

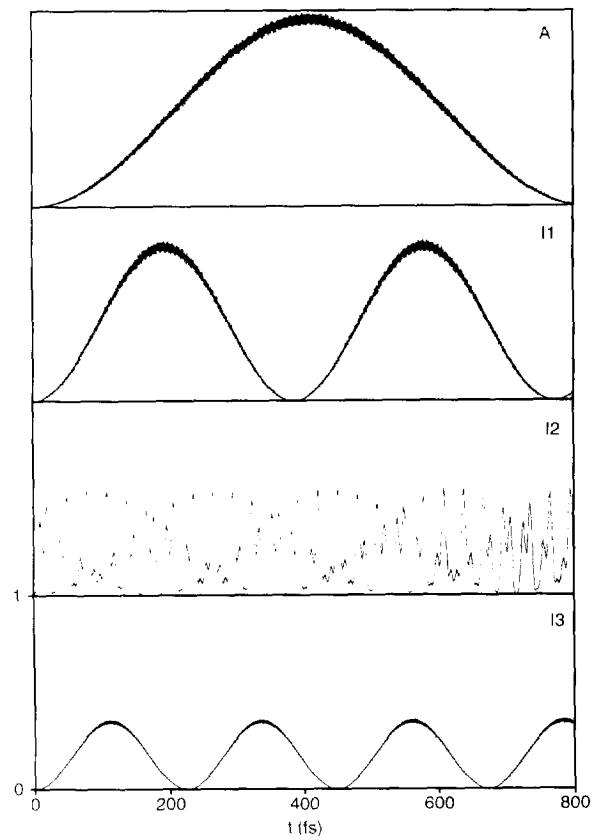

Fig. 16. $P_{N,1}(t)$ for the reference superexchange system **A**, and for the three impurity systems **I1**, **I2**, **I3**. The period of the dominant oscillation of $P_{N,1}(t)$ for each of the three impurity systems is smaller than the corresponding period for system **A**. The greatest reduction is observed for **I2**, where $P_{N,1}(t)$ consists of several competing oscillations of maximum period ≈ 20 fs.

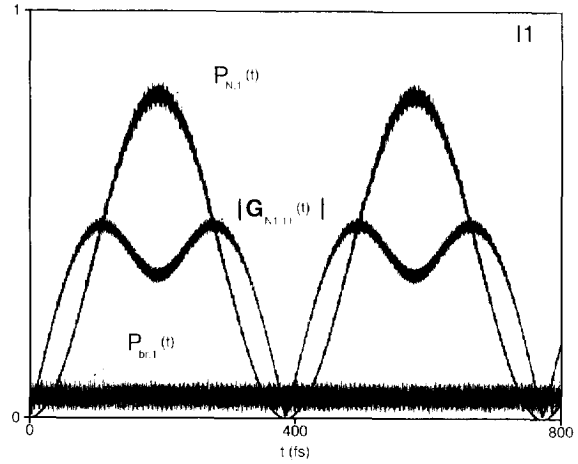

Fig. 17. Comparison of $P_{N,1}(t)$, $|G_{N1,11}(t)|$ (superexchange mechanism), and the total bridge population $P_{br,1}(t)$ (sequential mechanism), for system **I1**. $|G_{N1,11}(t)|$ is comparable to $P_{N,1}(t)$. $P_{br,1}(t)$ is negligible. This indicates that electron transfer takes place via a superexchange mechanism.

cillation as in the reference system, but with a shorter period (T_1: 800 fs → 400 fs). For **I2** $P_{N,1}(t)$ displays several competing oscillations with maximum period $T_1 \approx 20$ fs. E_{b_3} lies in an optimal regime and it induces a 40 fold reduction in the period of the major oscillation of $P_{N,1}(t)$ compared to the reference system **A**. In **I3** $P_{N,1}(t)$ displays only one major oscillation whose period has increased ($T_1 \approx 200$ fs) with respect to **I2**. This behaviour is understood by computing $R_{k_{im},i}$ ($i = 1, N$) for the different systems. One gets: $R_{k_{im},1} = 0.12$, $R_{k_{im},N} = 0.07$ (for I1), $R_{k_{im},1} = 4.05$, $R_{k_{im},N} = 1.82$ (for I2), and $R_{k_{im},1} = 0.04$, $R_{k_{im},N} = 0.01$ (for I3). The optimal regime observed for **I2** is due to the near resonance between $|k_{im}\rangle$ and $|1\rangle$, $|N\rangle$.

In Figs. 17, 18, 19 we plot $P_{N,1}(t)$, the magnitude of the superexchange matrix element $|G_{N1,11}(t)|$, and the total bridge population $P_{br,1}(t)$, for the three impurity systems (these quantities are shown for the reference system **A** in Fig. 7). For **I1** (Fig. 17) and **I3** (Fig. 19), $|G_{N1,11}(t)|$ dominates over $P_{br,1}(t)$, indicating superexchange electron transfer. In contrast, for **I2**, the sequential mechanism dominates over the superexchange. Figs. 18b and 18c show $|G_{N1,11}(t)|$ and $P_{br,1}(t)$ for **I2**. The amplitude of $P_{br,1}(t)$ is approximately twice that of $|G_{N1,11}(t)|$. The greatest contribution to $P_{br,1}(t)$ comes from the impurity eigenstate, as seen from $P_{k_{im},1}(t)$ in Fig. 18d. The impurity eigenstate has a large $|b_3\rangle$ component ($\langle b_3|k_{im}\rangle \approx 0.9$). Therefore, the contribution of the impurity site to $P_{br,1}(t)$ is also substantial (Fig. 18e).

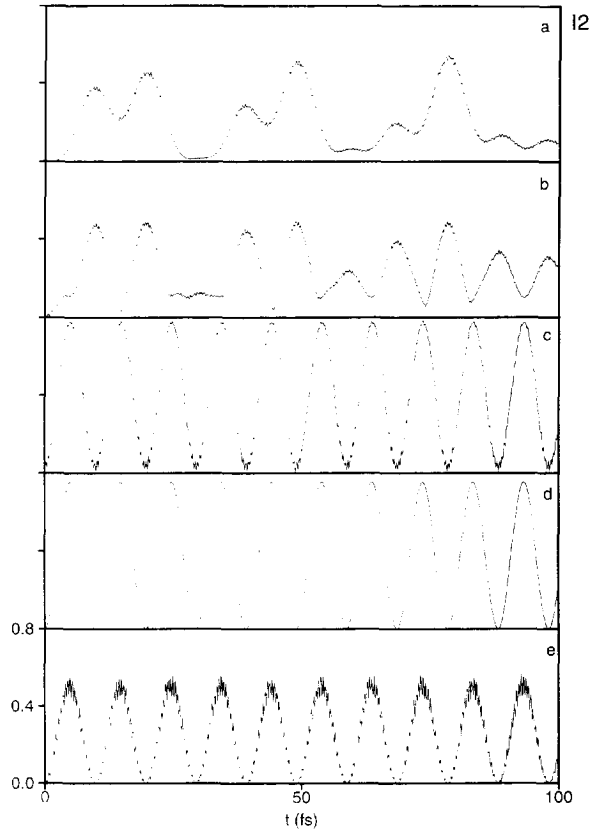

Fig. 18. Comparison of $P_{N,1}(t)$ (a), $|G_{N1,11}(t)|$ (b), $P_{br,1}(t)$ (c), $P_{k_{im},1}(t)$ (d), and $P_{b_3,1}(t)$ (e), for system **I2**. $P_{N,1}(t)$ and $|G_{N1,11}(t)|$ are of similar amplitude (≈ 0.45), and are both smaller than $P_{br,1}(t)$ (amplitude ≈ 0.8). This means that the sequential mechanism dominates. Most of $P_{br,1}(t)$ arises from $P_{k_{im},1}(t)$ (d). The contribution of the impurity site to $P_{br,1}(t)$ is substantial ($P_{b_3,1}(t)$ in (e)).

A more detailed view of the contribution of $|b_3\rangle$ to the superexchange and sequential mechanisms is obtained by plotting the entire density matrix in the local bridge basis, as a function of time (Fig. 20). The times chosen correspond to the maxima and minima of the major oscillations of $P_{N,1}(t)$. These plots indicate that the superexchange mechanism competes with the population of the impurity $|G_{b_3b_3,11}(t)|$, and more generally with $|G_{b_3i,11}(t)|$, $|G_{ib_3,11}(t)|$, ($i = 1, \ldots, N-2$). A similar plot of all $|G_{ij,11}(t)|$ for the reference superexchange system **A** is shown in Fig. 10.

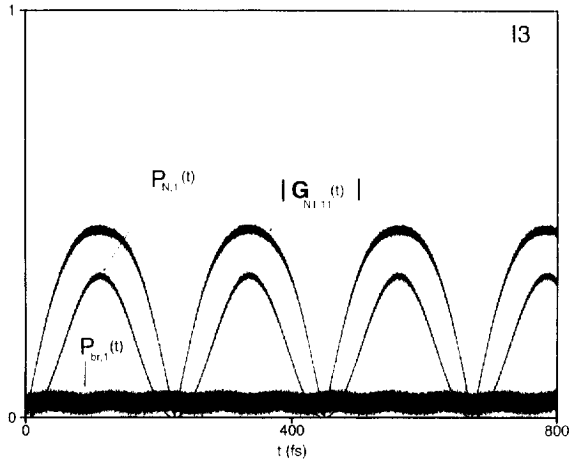

Fig. 19. Same as in Fig. 17 but for system I3. $|G_{N1,11}(t)|$ has slightly larger amplitude than $P_{N,1}(t)$, and both dominate over $P_{br,1}(t)$. The electron transfer is therefore superexchange.

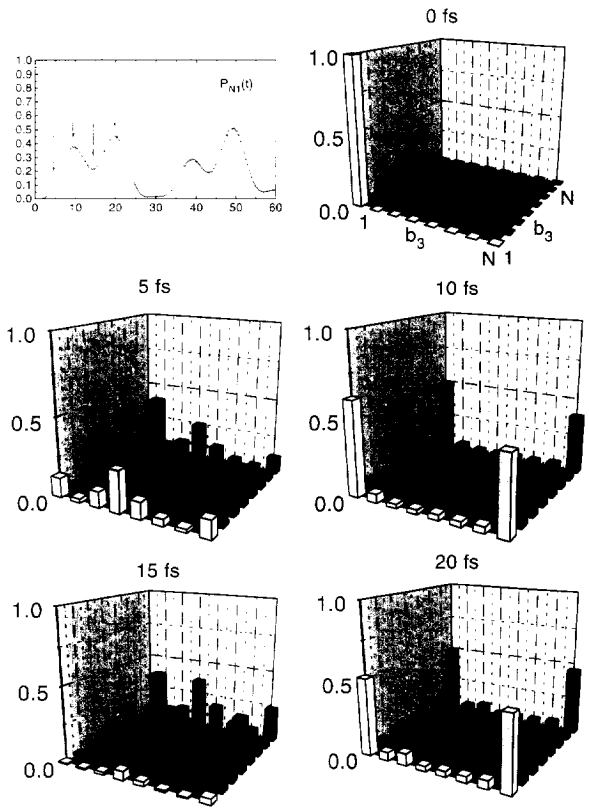

Fig. 20. Same as in Fig. 10 but for **I2**. The plots are at $t = 0$ and at several other times spanning the periods of the major oscillations of $P_{N,1}(t)$. The x and y axis of each plot label i and j in $|G_{ij,11}(t)|$, using the sequence 1, b_1, ... b_{N-2}, N. The impurity site b_3 is shown. The z axis gives the value of each $|G_{ij,11}(t)|$. The dominant matrix elements are $|G_{11,11}(t)| = P_{1,1}(t)$, $|G_{N1,11}(t)|$, $|G_{NN,11}(t)| = P_{N,1}(t)$, $|G_{b_3b_3,11}(t)| = P_{b_3,1}(t)$. The matrix elements $|G_{b_3i,11}(t)|$ $(i \neq b_3)$ are also large. These plots illustrate that the introduction of the impurity at b_3 enhances the sequential mechanism.

These calculations demonstrate that a significant reduction in the timescales of the dominant oscillations of $P_{N,1}(t)$ arises only if the bridge impurity site creates a bridge eigenstate that is near resonant to the donor and acceptor. In such a case the superexchange mechanism is inadequate. A Liouville space analysis should then be used to compute the superexchange and sequential contributions to $P_{N,1}(t)$. It is also possible that a reduction in the dominant oscillation timescales comes from a superexchange mechanism (cases I1 and I3 in Figs. 17 and 19). However, as seen in Fig. 16, this reduction is insignificant. Our discussion is relevant to systems where donor and acceptor involve p electrons (see, e.g., Refs. [45–47]). In these systems the electron transfer rate can be optimized by introducing π bonds in a section of the bridge. The optimal choice is when the π bonds create bridge eigenstates that are near resonant to donor and acceptor.

5. Discussion

In our model the impurity site is introduced in the middle of the bridge where it is not directly coupled to the donor or acceptor. The communication between donor, acceptor and impurity is via the intermediate bridge sites. This may well be the case in the photosynthetic reaction center where the coupling of the Bacteriochlorophyll monomer to the special pair or the Bacteriopheophytin could be mediated by the embedding protein. The variation of the impurity energy with respect to the donor and acceptor energies gives rise to different regimes of rate enhancement. One could imagine similar regimes occurring in the primary charge separation as the monomer's energy is varied. Optimal rate enhancement will occur if eigenstates of the monomer and the surrounding protein matrix are near resonant to the special pair and the Bacteriopheophytin. Therefore, any attempt to compute the energy of the "intermediate state" for the primary charge separation should consider the monomer

as well as the surrounding protein matrix. A three state model will oversimplify this dynamics since it condenses the combined effect of the Bacteriochlorophyll monomer and the surrounding protein to a single bridge state.

Liouville space pathways may provide a powerful tool for identifying the monomer's and the protein's contributions to the sequential and superexchange components of the rate. The present analysis focused on the purely electronic problem. It provides the basis for incorporating nuclear dynamics and inhomogeneous broadening which are important ingredients in determining the electron transfer rate. It is straightforward to include these effects if nuclear motions are either very fast or very slow compared with the rate. In the former case (homogeneous broadening), we can describe population relaxation and pure dephasing effects between any pair of states $|i\rangle$ and $|j\rangle$ $(i(j) = 1, N, k_m)$, by replacing $\hat{G}^0_{ii,jj}(\omega) = 1/(\omega - \omega_{i,j} + i\eta)$ by $1/(\omega - \omega_{ij} + if_{i,j})$, where $f_{i,j} = [(\gamma_i + \gamma_j)/2 + \Gamma_{i,j}]$. γ_i and γ_j describe population relaxation from states $|i\rangle$, $|j\rangle$, and $\Gamma_{i,j}$ describes pure dephasing. In the latter case, inhomogeneous broadening effects on superexchange and sequential contributions can be computed by numerical averaging of $G^{sup}_{NN,11}(\omega)$ and $G_{NN,11}(\omega) - G^{sup}_{NN,11}(\omega)$ over a distribution of site energies and/or intersite couplings. The incorporation of solvent motion with arbitrary time scale can be made using the path integral approach. The bath is then characterized by a spectral density which can be modelled using the multimode Brownian oscillator model [51]. Even for a system as simple as an alkyl chain it is difficult to guess the effect of the full nuclear dynamics on the rate. One can only identify nuclear motions that are important. For example, the local vibrations (stretching and rocking) of the C–C σ bonds alter the interbond couplings ($V_{i,j}$ in Eq. (3)). If the dominant oscillations of $P_{N,1}(t)$ (Fig. 16) compete with such vibrations (of periods $\lesssim$ ps), the effect on the rate could be significant.

We have demonstrated how the dynamics of the density matrix in Liouville space allows the computation of sequential corrections to the superexchange mechanism of electron transfer in the limit of strong coupling to the bridge. These corrections are significant when the donor and acceptor energies are close to the bridge eigenenergies. We have established the physical picture in these cases by looking at the time evolution of the full density matrix. The main advantage of the Liouville space analysis over the conventional Hilbert space representation is the clear separation of the superexchange and sequential components to the donor–acceptor transition probability.

In a Hilbert space analysis one approximates the energy splitting relevant to the electron transfer process by $H^{ef}_{N,1}(E_{tun})$. When the coupling between donor (acceptor) and bridge is increased, one has to vary E_{tun} in $H^{ef}_{N,1}(E_{tun})$ to a value that gives a good approximation to this splitting. This E_{tun} value may be very different from the donor and acceptor energies. However, we have demonstrated that no single choice of E_{tun} can describe strongly coupled systems where several energy splittings (time scales) dominate the electronic dynamics. For such systems one should retain the energy dependence of the effective two state Hamiltonian or construct effective Hamiltonians with more states. The importance of the sequential mechanism can then be deduced by comparing $P_{N,1}(t)$ to $P_{br,1}(t)$.

To identify and compute the superexchange and sequential contributions to $P_{N,1}(t)$, one has to resort to a density matrix analysis in Liouville space. The superexchange contributions are given by the effective two-state Liouville matrix elements $\Sigma_{11,11}(\omega)$, $\Sigma_{NN,NN}(\omega)$, $\Sigma_{NN,11}(\omega)$ (Eq. (A.7)). Similarly, the sequential contributions are given by $L^{ef}_{11,11}(\omega)$, $L^{ef}_{NN,NN}(\omega)$, $L^{ef}_{NN,11}(\omega)$ (Eq. (A.6)). These matrix elements enter the Fourier transform of $P_{N,1}(t)$, $(G_{NN,11}(\omega))$, and are written in terms of the Hilbert donor, acceptor and bridge states and energies. The effective two-state Liouville matrix elements are analogous to the effective two-state Hamiltonian matrix elements $H^{ef}_{1,1}(E)$, $H^{ef}_{N,N}(E)$, $H^{ef}_{N,1}(E)$ which enter the Fourier transform of $G_{N,1}(t)$ $(G_{N,1}(E))$. For the Hamiltonian case the expansion of $H^{ef}_{N,1}(E_{tun})$ in terms of bridge states gives the bridge pathways. Similarly, an expansion of $\Sigma_{ij,kl}(\omega)$ and $L^{ef}_{ij,kl}(\omega)$ in terms of the bridge states gives the Liouville space pathways. The advantage of the Liouville space pathway formulation is that one can distinguish between the pathways that contribute to the superexchange mechanism and the ones that contribute to the sequential mechanism (Figs. 6b and 6c). An interesting application of the present method will be for strongly

coupled donor–acceptor systems similar to those considered in Refs. [45–47], where the sequential contributions can be significant. For the primary charge separation this method can be used to distinguish the effects of the monomer and of the surrounding protein on the superexchange and sequential mechanisms. Indeed, as in Hilbert space pathway techniques, one can switch to localized bridge orbitals and visualize the superexchange and sequential contributions in terms of pathways that go through the protein matrix and the monomer. This will be of great value in the analysis of rate measurements of the primary charge separation using mutant reaction centers.

Acknowledgement

The support of the National Science Foundation and the Air Force office of scientific research is gratefully acknowledged.

Appendix A. Superexchange and sequential components to $G_{NN,11}(\omega)$

The Liouville space is partitioned into the subspaces

$$\Pi = P + Q_{\rm sup}\,, \quad \Lambda = Q_{\rm in} + Q_{\rm br}\,, \tag{A.1}$$

where the various projection operators are defined by

$$P = |11\rangle\rangle\langle\langle 11| + |NN\rangle\rangle\langle\langle NN|\,, \tag{A.2}$$

$$Q_{\rm in} = \sum_m \left(|k_m 1\rangle\rangle\langle\langle k_m 1| + |k_m N\rangle\rangle\langle\langle k_m N|\right) + \text{h.c.}\,,$$

$$Q_{\rm br} = \sum_{mn} |k_m k_n\rangle\rangle\langle\langle k_m k_n|\,,$$

$$Q_{\rm sup} = |N1\rangle\rangle\langle\langle N1| + |1N\rangle\rangle\langle\langle 1N|\,. \tag{A.3}$$

The subscripts "in", "br", and "sup", stand for "intermediate", "bridge", and "superexchange". This partitioning gives

$$\Pi\hat{\mathsf{G}}(\omega)\Pi = \Pi\frac{1}{\omega - \Pi\hat{\mathsf{L}}^{\rm ef}(\omega)\Pi}\Pi\,, \tag{A.4}$$

where

$$\hat{\mathsf{L}}^{\rm ef}(\omega) = \hat{\mathsf{L}}\Lambda\frac{1}{\omega - \Lambda\hat{\mathsf{L}}\Lambda}\Lambda\hat{\mathsf{L}}\,. \tag{A.5}$$

$\Pi\hat{\mathsf{L}}^{\rm ef}(\omega)\Pi$ is a 4×4 matrix and it can be written in terms of the bridge eigenstates $|k_m\rangle$:

$$\Pi\hat{\mathsf{L}}^{\rm ef}(\omega)\Pi = \Pi\hat{\mathsf{L}}Q_{\rm in}\left\{\omega - Q_{\rm in}\hat{\mathsf{L}}Q_{\rm in} - Q_{\rm in}\hat{\mathsf{L}}Q_{\rm br}\frac{1}{\omega - Q_{\rm br}\hat{\mathsf{L}}Q_{\rm br}}Q_{\rm br}\hat{\mathsf{L}}Q_{\rm in}\right\}^{-1}Q_{\rm in}\hat{\mathsf{L}}\Pi\,.$$

Since we are interested in level populations we express $G_{NN,11}(\omega)$ in terms of the 2×2 matrix

$$P\hat{\mathsf{G}}(\omega)P = P\frac{1}{w - P\hat{\mathsf{L}}^{\rm ef}(\omega)P - P\hat{\Sigma}(\omega)P}P\,. \tag{A.6}$$

$P\hat{\Sigma}(\omega)P$ is the superexchange contribution given by

$$P\hat{\Sigma}(\omega)P = P\hat{\mathsf{L}}^{\rm ef}(\omega)Q_{\rm sup}\times\frac{1}{w - Q_{\rm sup}\hat{\mathsf{L}}^{\rm ef}(\omega)Q_{\rm sup}}Q_{\rm sup}\hat{\mathsf{L}}^{\rm ef}(\omega)P, \tag{A.7}$$

and $P\hat{\mathsf{L}}^{\rm ef}(\omega)P$ is the sequential contribution (does not involve states $|N1\rangle\rangle$, $|1N\rangle\rangle$). The superexchange Green function is defined as

$$P\hat{\mathsf{G}}^{\rm sup}(\omega)P \equiv P\frac{1}{\omega - P\hat{\Sigma}(\omega)P}P. \tag{A.8}$$

The relevant matrix element of $P\hat{\mathsf{G}}^{\rm sup}(\omega)P$ is

$$\mathsf{G}^{\rm sup}_{NN,11}(\omega) = \Sigma_{NN,11}(\omega)\times\left\{\left[\omega - \Sigma_{11,11}(\omega)\right]\left[\omega - \Sigma_{NN,NN}(\omega)\right] - \Sigma_{NN,11}(\omega)\Sigma_{11,NN}(\omega)\right\}^{-1}. \tag{A.9}$$

The total $G_{NN,11}(\omega)$ is now expressed in terms of $P\hat{\mathsf{G}}^{\rm sup}(\omega)P$ and the tetradic scattering matrix $P\hat{\mathsf{T}}^{\rm seq}(\omega)P$ arising from the sequential matrix elements $P\hat{\mathsf{L}}^{\rm ef}(\omega)P$. The relation between $P\hat{\mathsf{G}}(\omega)P$, $P\hat{\mathsf{G}}^{\rm sup}(\omega)P$, and the scattering matrix

$$P\hat{\mathsf{G}}(\omega)P = P\hat{\mathsf{G}}^{\rm sup}(\omega)P + P\hat{\mathsf{G}}^{\rm sup}(\omega)P\left[P\hat{\mathsf{T}}^{\rm seq}(\omega)P\right]P\hat{\mathsf{G}}^{\rm sup}(\omega)P\,, \tag{A.10}$$

where the scattering matrix $P\hat{\mathsf{T}}^{\mathrm{seq}}(\omega)P$ is given by

$$P\hat{\mathsf{T}}^{\mathrm{seq}}(\omega)P = P\hat{\mathsf{L}}^{\mathrm{ef}}(\omega)P + P\hat{\mathsf{L}}^{\mathrm{ef}}(\omega)P\left[P\hat{\mathsf{G}}(\omega)P\right]P\hat{\mathsf{L}}^{\mathrm{ef}}(\omega)P. \quad (A.11)$$

Solving for $P\hat{\mathsf{T}}^{\mathrm{seq}}(\omega)P$ in terms of $P\hat{\mathsf{G}}^{\mathrm{sup}}(\omega)P$ and $P\hat{\mathsf{L}}^{\mathrm{ef}}(\omega)P$ gives

$$P\hat{\mathsf{T}}^{\mathrm{seq}}(\omega)P = P\frac{1}{I - P\hat{\mathsf{L}}^{\mathrm{ef}}(\omega)\hat{\mathsf{G}}^{\mathrm{sup}}(\omega)P}P\hat{\mathsf{L}}^{\mathrm{ef}}(\omega)P. \quad (A.12)$$

The final result is

$$\mathsf{G}_{NN,11}(\omega) = \mathsf{G}^{\mathrm{sup}}_{NN,11}(\omega) + \sum_{\alpha\beta,\gamma\delta=11,NN}\mathsf{G}^{\mathrm{sup}}_{NN,\alpha\beta}(\omega)\mathsf{T}^{\mathrm{seq}}_{\alpha\beta,\gamma\delta}(\omega)\mathsf{G}^{\mathrm{sup}}_{\gamma\delta,11}(\omega), \quad (A.13)$$

where

$$\mathsf{T}^{\mathrm{seq}}_{11,11}(\omega) = \frac{1}{1-\Phi(\omega)}\times\left[\mathsf{L}^{\mathrm{ef}}_{11,11}(\omega) - \mathsf{G}^{\mathrm{sup}}_{NN,NN}(\omega)\det[P\hat{\mathsf{L}}^{\mathrm{ef}}(\omega)P]\right], \quad (A.14)$$

$$\mathsf{T}^{\mathrm{seq}}_{NN,NN}(\omega) = \frac{1}{1-\Phi(\omega)}\times\left[\mathsf{L}^{\mathrm{ef}}_{NN,NN}(\omega) - \mathsf{G}^{\mathrm{sup}}_{11,11}(\omega)\det[P\hat{\mathsf{L}}^{\mathrm{ef}}(\omega)P]\right], \quad (A.15)$$

$$\mathsf{T}^{\mathrm{seq}}_{NN,11}(\omega) = \frac{1}{1-\Phi(\omega)}\times\left[\mathsf{L}^{\mathrm{ef}}_{NN,11}(\omega) + \mathsf{G}^{\mathrm{sup}}_{NN,11}(\omega)\det[P\hat{\mathsf{L}}^{\mathrm{ef}}(\omega)P]\right], \quad (A.16)$$

$$\mathsf{T}^{\mathrm{seq}}_{11,NN}(\omega) = \frac{1}{1-\Phi(\omega)}\times\left[\mathsf{L}^{\mathrm{ef}}_{11,NN}(\omega) + \mathsf{G}^{\mathrm{sup}}_{11,NN}(\omega)\det[P\hat{\mathsf{L}}^{\mathrm{ef}}(\omega)P]\right], \quad (A.17)$$

$$\Phi(\omega) = \mathsf{L}^{\mathrm{ef}}_{11,11}(\omega)\mathsf{G}^{\mathrm{sup}}_{11,11}(\omega) + \mathsf{L}^{\mathrm{ef}}_{NN,NN}(\omega)\mathsf{G}^{\mathrm{sup}}_{NN,NN}(\omega) + \mathsf{L}^{\mathrm{ef}}_{NN,11}(\omega)\mathsf{G}^{\mathrm{sup}}_{11,NN}(\omega) + \mathsf{L}^{\mathrm{ef}}_{11,NN}(\omega)\mathsf{G}^{\mathrm{sup}}_{NN,11}(\omega) - \det[P\hat{\mathsf{L}}^{\mathrm{ef}}(\omega)P]\times\det[P\hat{\mathsf{G}}_{\mathrm{sup}}(\omega)P]. \quad (A.18)$$

Appendix B. Alternative partitioning of $\mathsf{G}_{NN,11}(\omega)$

The definition of superexchange given in Appendix A and used throughout this work requires that a superexchange process visits states $|N1\rangle\rangle$, $|1N\rangle\rangle$. However, these states can be visited via $|k_mk_n\rangle\rangle$, as seen from Eqs. A.6, A.7. An alternative partitioning of $\mathsf{G}_{NN,11}(\omega)$ is obtained by defining as superexchange any process contributing to the transition from $|11\rangle\rangle$ to $|NN\rangle\rangle$ that does not visit bridge populations and coherences $|k_mk_n\rangle\rangle$. The Liouville space is partitioned into the subspaces:

$$P = |11\rangle\rangle\langle\langle 11| + |NN\rangle\rangle\langle\langle NN|,$$

$$Q_{\mathrm{in}} = \sum_m\left(|k_m1\rangle\rangle\langle\langle k_m1| + |k_mN\rangle\rangle\langle\langle k_mN|\right) + \mathrm{c.c.},$$

$$Q_{\mathrm{br}} = \sum_{mn}|k_mk_n\rangle\rangle\langle\langle k_mk_n|,$$

$$Q_{\mathrm{sup}} = |N1\rangle\rangle\langle\langle N1| + |1N\rangle\rangle\langle\langle 1N|. \quad (B.1)$$

This partitioning gives

$$P\hat{\mathsf{G}}(\omega)P = P\frac{1}{\omega - P\hat{R}(\omega)P}P, \quad (B.2)$$

where

$$P\hat{R}(\omega)P = P\hat{\mathsf{L}}Q_{\mathrm{in}}\left\{\omega - Q_{\mathrm{in}}\hat{\mathsf{L}}Q_{\mathrm{in}} - Q_{\mathrm{in}}\hat{R}_{\mathrm{sup}}(\omega)Q_{\mathrm{in}} - Q_{\mathrm{in}}\hat{R}_{\mathrm{seq}}(\omega)Q_{\mathrm{in}}\right\}^{-1}Q_{\mathrm{in}}\hat{\mathsf{L}}P, \quad (B.3)$$

and

$$Q_{\mathrm{in}}\hat{R}_{\mathrm{sup}}(\omega)Q_{\mathrm{in}} = Q_{\mathrm{in}}\hat{\mathsf{L}}Q_{\mathrm{sup}}\frac{1}{\omega - Q_{\mathrm{sup}}\hat{\mathsf{L}}Q_{\mathrm{sup}}}Q_{\mathrm{sup}}\hat{\mathsf{L}}Q_{\mathrm{in}},$$

$$Q_{\mathrm{in}}\hat{R}_{\mathrm{seq}}(\omega)Q_{\mathrm{in}} = Q_{\mathrm{in}}\hat{\mathsf{L}}Q_{\mathrm{br}}\frac{1}{\omega - Q_{\mathrm{br}}\hat{\mathsf{L}}Q_{\mathrm{br}}}Q_{\mathrm{br}}\hat{\mathsf{L}}Q_{\mathrm{in}}. \quad (B.4)$$

$Q_{\mathrm{in}}\hat{R}_{\mathrm{sup}}(\omega)Q_{\mathrm{in}}$ and $Q_{\mathrm{in}}\hat{R}_{\mathrm{seq}}(\omega)Q_{\mathrm{in}}$ are the superexchange and sequential contributions. The superexchange Green function is defined as

$$P\hat{G}_{\mathrm{sup}}(\omega)P = P\Big\{\omega - P\hat{L}Q_{\mathrm{in}} \times \frac{1}{\omega - Q_{\mathrm{in}}\hat{L}Q_{\mathrm{in}} - Q_{\mathrm{in}}\hat{R}_{\mathrm{sup}}(\omega)Q_{\mathrm{in}}} Q_{\mathrm{in}}\hat{L}P\Big\}^{-1} P. \tag{B.5}$$

$P\hat{G}_{\mathrm{sup}}(\omega)P$ is different from $P\hat{G}^{\mathrm{sup}}(\omega)P$ in Eq. (A.8) since it excludes the states $|k_m k_n\rangle\rangle$.

References

[1] R.A. Marcus and N. Sutin, Biochim. Biophys. Acta 811 (1985) 265.
[2] M.A. Fox, M. Chanon, eds, Photoinduced electron transfer (Elsevier, Amsterdam, 1989).
[3] M.R. Wasielewski, Chem. Rev. 92 (1992) 435.
[4] D. Gust, T.A. Moore and L.A. Moore, Accounts Chem. Res. 26 (1993) 198.
[5] C.C. Moser, J.M. Keske, K. Warncke, R.S. Farid and P.L. Dutton, Nature 355 (1992) 796.
[6] J. Bolton, G.L. McLendon and N. Mataga, eds., ACS Advan. Chem. Ser., Vol. 228. Electron transfer in inorganic, organic, and biological systems (American Chemical Society, Washington, 1991.
[7] H.M. McConnell J. Chem. Phys. 35 (1961) 508.
[8] P.O. Löwdin, J. Math. Phys. 3 (1962) 969.
[9] S. Larsson, J. Am. Chem. Soc. 103 (1981) 4034; J. Chem. Soc. Faraday Trans. II 79 (1983) 1375.
[10] R.A. Marcus, J. Chem. Phys. 24 (1956) 979; 43 (1965) 679.
[11] N.S. Hush, Trans. Faraday Soc. 57 (1961) 155; Electrochim. Acta 13 (1968) 1005.
[12] J.J. Hopfield, Proc. Natl. Acad. Sci. USA 71 (1974) 3640.
[13] J. Jortner, J. Chem. Phys. 64 (1976) 4860;
M. Bixon and J. Jortner, J. Chem. Phys. 48 (1968) 715; 50 (1969) 3284.
[14] S.S. Skourtis, D.N. Beratan and J.N. Onuchic, Chem. Phys. 176 (1993) 501;
S.S. Skourtis and J.N. Onuchic, Chem. Phys. Letters 209 (1993) 171.
[15] G. Feher, J.P. Allen, M.Y. Okamura and D.C. Rees, Nature 339 (1989) 111.
[16] J. Deisenhofer and H. Michel, EMBO J. 8 (1989) 2149.
[17] J.P. Allen, G. Feher, T.O. Yeates, J. Deisenhofer, H. Michel and R. Huber, Proc. Natl. Acad. Sci. USA 83 (1986) 8589.
[18] M. Bixon, J. Faher, G. Feher, J.H. Freed, D. Gamliel, A.J. Hoff, H. Levanon, K. Möbius, R. Nechustai, J.R. Norris, A. Scherz, J.L. Sessler and D. Stehlik, Israel J. Chem. (1992) 32.
[19] G.J. Small, J.M. Hayes and R.J. Silbey, J. Phys. Chem. 96 (1992) 7499.
[20] A. Warshel and W.W. Parson, Annu. Rev. Phys. Chem. 42 (1991) 279.
[21] N. Marchi, J.N. Gehlen, D. Chandler and M. Newton, J. Am. Chem. Soc. 115 (1993) 4178.
[22] S.G. Johnson, D. Tang, R. Jankowiak, J.M. Hayes, G.J. Small and D.M. Tiede, J. Phys. Chem. 94 (1990) 5849.
[23] M.H. Vos, J.C. Lambry, S.J. Robles, D.C. Youvan, J. Breton and J.L. Martin, Proc. Natl. Acad. Sci. USA 88 (1991) 8885.
[24] D.J. Lockhart and S.G. Boxer, Chem. Phys. Letters 144 (1988) 243;
D.J. Lockhart, C. Kirmaier, D. Holten and S.G. Boxer, J. Phys. Chem. 94 (1990) 6987;
T.R. Middendorf, L.T. Mazzola, D.F. Gaul, C.C. Schenck and S.G. Boxer, J. Phys. Chem. 95 (1991) 10142;
A.P. Shreve, N.J. Cherepy, S. Franzen, S.G. Boxer and R.A. Mathies, Proc. Natl. Acad. Sci. USA 88 (1991) 11207.
[25] G.R. Fleming, J.L. Martin and J. Breton, Nature 333 (1988) 190.
[26] W. Holzapfel, U. Finkele, W. Kaiser, D. Oesterheldt, H. Scheer, U. Stilz and W. Zinth, Chem. Phys. Letters 160 (1989) 1; Proc. Natl. Acad. Sci. USA 87 (1990) 5168;
S. Schmidt, T. Arlt, P. Hamm, H. Huber, T. Nagele, J. Wachtveitl, M. Meyer, H. Scheer and W. Zinth, Chem. Phys. Letters 223 (1994) 116.
[27] D. Holten and C. Kirmaier, Proc. Natl. Acad. Sci. USA 87 (1990) 3522;
C. Kirmaier and D. Holten, Biochemistry 30 (1991) 609.
[28] J.M. Jean, R.A. Friesner and G.R. Fleming, J. Chem. Phys. 96 (1992) 5827.
[29] S.S. Skourtis, A.J. da Silva, W. Bialek and J.N. Onuchic, J. Phys. Chem. 96 (1992) 8034.
[30] J.S. Joseph and W.A. Bialek, J. Phys. Chem 97 (1993) 3245.
[31] J. Tang, Z. Wang and J.R. Norris, J. Chem. Phys. 99 (1993) 979.
[32] R. Egger and C.H. Mak, J. Phys. Chem. 98 (1994) 9903.
[33] Yu. Hu and S. Mukamel, J. Chem. Phys. 91 (1989) 6973; Chem. Phys. Letters 160 (1989) 410;
J. Jortner and P. Pullman, eds., Perspectives in photosynthesis (Kluwer, Dordrecht, 1989) p. 171.
[34] M. Bixon, J. Jortner, M.E. Michel-Beyerle and A. Ogrodnik, Biochim. Biophys. Acta 977 (1989) 273;
M. Bixon, J. Jortner and M.E. Michel-Beyerle, Biochim. Biophys. Acta 1056 (1991) 301.
[35] J.J. Regan, S.M. Risser, D.N. Beratan and J.N. Onuchic, J. Phys. Chem. 97 (1993) 13083;
D.N. Beratan, J.N. Betts and J.N. Onuchic, Science 252 (1991) 1285;
J.N. Onuchic, P.C.P. de Andrade and D.N. Beratan, J. Chem. Phys. 95 (1991) 1131;
D.N. Beratan, J.N. Onuchic and J.J. Hopfield, J. Chem. Phys. 86 (1987) 4488; 83 (1985) 5325;
D.N. Beratan and J.J. Hopfield, J. Am. Chem. Soc. 106 (1984) 1584.
[36] S.S. Skourtis, J.J. Regan and J.N. Onuchic, J. Phys. Chem. 98 (1994) 3379.
[37] M.J. Therien, B.E. Bowler, M.A. Selman, H.B. Gray, I.-J.Chang and J.R. Winkler, in: ACS Advan. Chem. Ser., Vol. 228. Electron transfer in inorganic, organic, and biological systems, eds. J. Bolton, G.L. McLendon and N. Mataga

(American Chemical Society, Washington, 1991) p. 191;
M.J. Therien, M.A. Selman, H.B. Gray, I.-J. Chang and J.R. Winkler, J. Am. Chem. Soc. 112 (1990) 2420;
D.S. Wuttke, M.J. Bjerrum, J.R. Winkler and H.B. Gray, Science 256 (1992) 1007;
D.S. Wuttke, M.J. Bjerrum, I.-J.Chang, J.R. Winkler and H.B. Gray, Biochim. Biophys. Acta 1101 (1992) 168;
D.R. Casimiro, L.L. Wong, J.L. Colon, T.E. Zewert, J.H. Richards, I.-J. Chang, J.R. Winkler and H.B. Gray, J. Am. Chem. Soc. 115 (1993) 1485.

[38] G. McLendon and R. Hake, Chem. Rev. 92 (1992) 481;
G. McLendon, Accounts Chem. Res. 21 (1988) 160.

[39] O. Farver and I. Pecht, J. Am. Chem. Soc. 114 (1992) 5764; Faseb. J. 5 (1991) 2554;
D.W. Conrad, H. Zhang, D.E. Stewart and R.A. Scott, J. Am. Chem. Soc. 114 (1992) 9909.

[40] A.A.S. da Gama, J. Theoret. Biol. 142 (1990) 251;
M.A. Ratner, J. Phys. Chem. 94 (1990) 4877;
C. Goldman, Phys. Rev. A 43 (1991) 4500;
J. Malinsky and Y. Magarshak, J. Phys. Chem. 92 (1992) 2849;
J.W. Evenson and M. Karplus, J. Chem. Phys., 96 (1992) 5272;
V. Mujica, M. Kemp and M.A. Ratner, J. Chem. Phys. 8 (1994) 6849;
V. Mujica, M. Kemp and M.A. Ratner, J. Chem. Phys. 8 (1994) 6856.

[41] A. Kuki and P.G. Wolynes, Science 236 (1987) 1647.

[42] J.M. Gruschus and A. Kuki, J. Phys. Chem. 97 (1993) 5581

[43] P. Siddarth and R.A. Marcus, J. Phys. Chem. 97 (1993) 6112, 2400.

[44] S. Larsson, Chem. Scr. 28A (1988) 15;
S. Larsson, A. Broo, B. Kallebring and A. Volosov, Intern. J. Quantum Chem. S15 (1988) 1;
A. Broo and S. Larsson, J. Phys. Chem. 95 (1991) 4925;
H.E.M. Christensen, L.S. Conrad, K.V. Mikkelsen, M.K. Nielsen and J. Ulstrup, J. Inorg. Chem. 29 (1990) 2808.

[45] M.D. Newton, Chem. Rev. 91 (1991) 767;
C. Liang and M.D. Newton, J. Phys. Chem. 96 (1992) 2855.

[46] L.A. Curtiss, C.A. Naleway and J.R. Miller, Chem. Phys. 176 (1993) 387;
C.A. Naleway, L.A. Curtiss and J.R. Miller, J. Phys. Chem. 95 (1991) 8434.

[47] K.D. Jordan and M.N. Paddon-Row, J. Phys. Chem. 96 (1992) 1188; Chem. Rev. 92 (1992) 395.

[48] M. Sparpaglione and S. Mukamel, J. Chem. Phys 88 (1988) 3263, 4300.

[49] S. Mukamel and Y.J. Yan, Accounts Chem. Res. 22 (1989) 301;
Y.J. Yan and S. Mukamel, J. Phys. Chem. 93 (1989) 6991.

[50] S. Mukamel, Advan. Chem. Phys. 70, Part I (1988) 165.

[51] S. Mukamel, Principles of nonlinear optical spectroscopy (Oxford Univ. Press, New York, 1995).

[52] R. Egger, C.H. Mak and U. Weiss, Phys. Rev. E 50 (1994) R655.

[53] Y. Tanimura and S. Mukamel, Phys. Rev. E 47 (1993) 118; J. Chem. Phys. 101 (1994) 3049.

[54] A. Ben-Reuven and S. Mukamel, J. Phys. A 8 (1975) 1313.

[55] J.W. Evenson and M. Karplus, Science 262 (1993) 1247.

[56] U. Fano, Rev. Mod. Phys. 29 (1957) 74; 45 (1974) 553.

[57] R. Zwanzig, Lectures Theoret. Phys. 3 (1961) 106; Physica 30 (1964) 1109.

[58] M.E. Winfield, J. Mol. Biol. 12 (1965) 600;
T. Takano, O.B. Kallai, R. Swanson and R.E. Dickerson, J. Biol. Chem. 248 (1973) 5234.

[59] J.N. Onuchic and D.N. Beratan, J. Chem. Phys. 92 (1990) 722.

[60] D.E. Richardson and H. Taube, J. Am. Chem. Soc. 105 (1983) 40;
D. Heiler, G. McLendon and P. Rogalskji, J. Am. Chem. Soc. 109 (1987) 604;
H. Heitele and M.E. Michel-Beyerle J. Am. Chem. Soc. 107 (1985) 8286.